CRYSTAL GROWTH & DESIGN

Article

pubs.acs.org/crystal

Contrasting Polymorphism of Related Small Molecule Drugs Correlated and Guided by the Computed Crystal Energy Landscape

Doris E. Braun,*[,†,‡] Jennifer A. McMahon,[§] Lien H. Koztecki,[§] Sarah L. Price,[†] and Susan M. Reutzel-Edens[§]

[†]Department of Chemistry, University College London, 20 Gordon Street, London WC1H 0AJ, U.K.

[‡]Institute of Pharmacy, University of Innsbruck, Innrain 52c, 6020 Innsbruck, Austria

[§]Eli Lilly and Company, Indianapolis, Indiana 46285, United States

Supporting Information

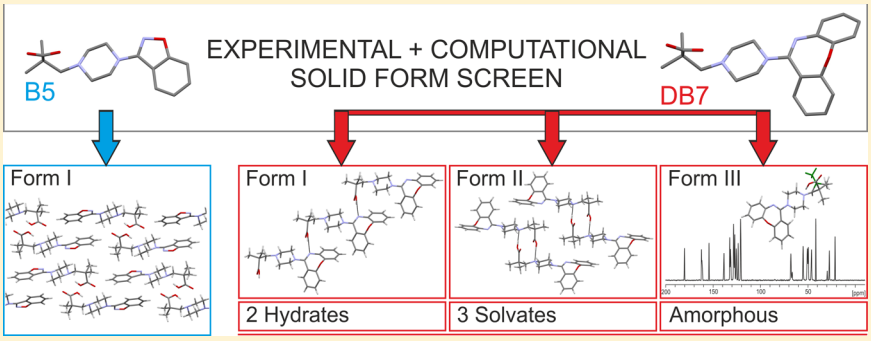

ABSTRACT: Solid form screening and crystal structure prediction (CSP) calculations were carried out on two related molecules, 3-(4-(benzo[d]isoxazole-3-yl)piperazin-1-yl)-2,2-dimethylpropanoic acid (B5) and 3-(4-dibenzo[b,f][1,4]oxepin-11-yl-piperazin-1-yl)-2,2-dimethylpropanoic acid (DB7). Only one anhydrate form was crystallized for B5, whereas multiple solid forms, including three neat polymorphs, were found for DB7. The crystal structure of B5 is $P2_1/n$ $Z' = 1$ with intramolecular hydrogen bonding, whereas Forms I and II of DB7 are conformational polymorphs with distinct $Z' = 1$ $P\bar{1}$ structures and intermolecular hydrogen bonds. A disordered structure for Form III of DB7 is proposed, based on CSP-generated structures which gave a promising match to the X-ray powder diffraction and solid state NMR data for this metastable form. The differences in the hydrogen bonding and experimental solid form landscapes of the two molecules appear to arise from the dominance of the self-assembly of the benzoisoxazolepiperazinyl and dibenzoxepinylpiperazinyl fragments and the consequent inability to produce amorphous or solvate forms as intermediates for B5. There is a subtle balance between the intramolecular conformational energy and the intermolecular dispersion, electrostatic and polarization interactions apparent in the analysis of the computationally generated thermodynamically competitive structures, which makes their relative stability quite sensitive to the computational method used. The value of simultaneously exploring the computationally and experimentally generated solid form landscapes of molecules in pharmaceutical development is discussed.

1. INTRODUCTION

Multidisciplinary solid form screening[1−3] is routinely conducted in the pharmaceutical and specialty chemicals industries to ensure that solid forms with the best compromise of physical and chemical properties are developed. Reports of the late appearance of polymorphs[4,5] and the wide range of methods that have led to the discovery of novel polymorphs[6] show, however, that there is no standard recipe for comprehensive experimental solid form screening. With neither a sure fire approach nor a clear end point to finding crystal forms, a computational method for ensuring that all relevant polymorphs have been found is highly desirable. To this end, studies on smaller molecules have established crystal structure prediction (CSP) as a complement to solid form screening,[7−11] helping to rationalize and unify experimental observations on polymorphs, solvates, and hydrates.[12−16] In the most recent (2010) blind test of CSP methods, the progress toward tackling larger, flexible molecules allowed a target crystal structure of a molecule large enough to be seen as a model for modern smaller drug molecules.[17] The success in predicting the crystal structure of blind test candidate benzyl-(4-(4-methyl-5-(*p*-tolylsulfonyl)-1,3-thiazol-2-yl)phenyl)carbamate (XX)[18] has led to a series of studies in which the crystal energy landscapes of pharmaceuticals, such as olanzapine (LY170053),[19] *N*-[(2*R*)-(6-chloro-5-methoxy-1*H*-indol-3-yl)-propyl]acetamide (melatonin agonist, LY156735),[9,10] and 6-[(5-chloro-2-([(4-chloro-2-fluorophenyl)methyl]oxy)phenyl)methyl]-2-pyridinecarboxylic acid (GSK269984B),[20] have been contrasted with industrial

Received: February 4, 2014
Revised: March 5, 2014
Published: March 5, 2014

experimental screening work and used to focus additional investigations to give an overall picture of each molecule's experimental solid form landscape. In this study, we seek to contrast the crystallization behavior and crystal energy landscapes of two molecules, which were part of the same drug discovery program, and show how the solid form landscape varies with minor chemical modifications to the API.[21] This shows the extent to which the pharmaceutical materials tetrahedron,[22] the relationships between the possible structures, properties, performance, and processing, is specific to a given API rather than a family, and the potential role of CSP in providing the required information.

The first molecule, 3-(4-(benzo[d]isoxazole-3-yl)piperazin-1-yl)-2,2-dimethylpropanoic acid (LY2806920, B5, Figure 1a), is

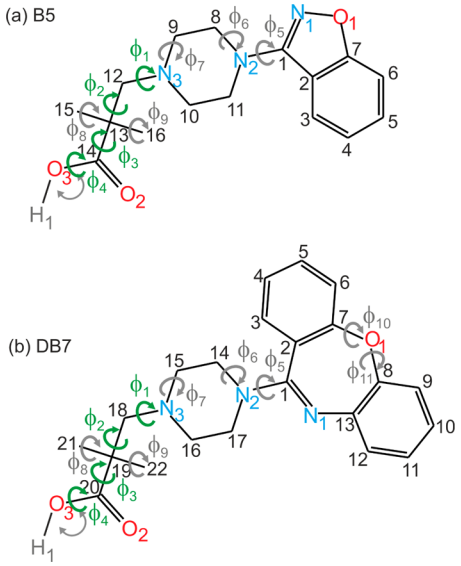

Figure 1. (a, b) The related molecules being studied, with atomic numbering. The abbreviated names B5 and DB7 refer to the different size and identity of rings comprising the benzoisoxazole and dibenzoxepinyl ring systems. The highly flexible intramolecular degrees of freedom that were explicitly varied in the CrystalPredictor search procedure are in green (ϕ_1: C9−N3−C12−C13, ϕ_2: N3−C12−C13−C14, ϕ_3: C12−C13−C14−O3, ϕ_4: C13−C14−O3−H1, with B5 numbering, corresponding angles used for DB7), with gray showing the additional angles that were also included in the final CrystalOptimizer refinement.

a 5-HT$_{2a}$ agonist that was investigated for the oral treatment of depression and sleep disorders, while the second, 3-(4-dibenzo[b,f][1,4]oxepin-11-yl-piperazin-1-yl)-2,2-dimethylpropanoic acid (LY2624803, DB7, Figure 1b), is a 5-HT$_{2a}$ agonist and H1 inverse agonist that was under development as an oral treatment for both sleep onset and sleep maintenance. Both molecules are amphoteric, capable of existing in zwitterionic and charge neutral forms, and have the same hydrogen bonding groups. Work on screening the two compounds revealed contrasting solid form behavior, with B5 showing only one nonsolvated solid form and DB7 crystallizing in at least three neat polymorphs and multiple hydrates and solvates. Both B5 and DB7 were un-ionized in the observed nonsolvated crystal forms, but the hydrogen bonding of the common part of the molecules was different. Whereas B5 was intramolecularly hydrogen bonded in its only solid form, DB7 formed intermolecular hydrogen bonds in the two readily structurally characterized anhydrates.

The initial indication of very different solid form diversity between these molecules with a great deal of chemical and pharmacological similarity led us to calculate the crystal energy landscapes of the two molecules with the aim of assessing (i) whether it could account for the differences in crystallization behavior, (ii) whether it could propose a structure for DB7 Form III, which had not been structurally characterized by single crystal diffraction for lack of suitable crystals and (iii) whether the calculations would suggest further experimental work to characterize the solid form diversity of these molecules. More generally, the goal of the project was to learn how to usefully incorporate CSP into an industrial solid form screening process, given recent extension of the capability for these size molecules.

2. MATERIALS AND METHODS

2.1. Computational Generation of the Crystal Energy Landscapes and Lattice Energy Calculations. The CSP search[23] for low energy structures of the two neutral molecules was based on separately calculating the intermolecular lattice energy, U_{inter}, and the intramolecular energy penalty, ΔE_{intra}, for changing the conformation of the molecule. The static lattice energy of a crystal, $E_{latt} = U_{inter} + \Delta E_{intra}$, is calculated from increasingly accurate estimates of ΔE_{intra}, based on electronic structure calculations on the molecules, and improving the quality of the atom−atom model for the intermolecular forces for U_{inter}. The plausible range of conformational flexibility for molecules B5 and DB7 which needed to be covered in the CrystalPredictor search (Figure 1) was established by potential energy surface scans and analyses of the Cambridge Structural Database[24] (Supporting Information section 1). These showed that three flexible CrystalPredictor[25−27] searches were appropriate, corresponding to three different carboxylic acid conformations with either $\phi_4 = 180°$ (for intermolecular hydrogen bonds) or $\phi_4 = 0°$ giving an intramolecular hydrogen bond, with two different regions (iA and iB searches, Figure 2). The other dimethylpropanoic acid angles (ϕ_1−ϕ_3) were included as search variables, and ϕ_5 was fixed to 50.9° for B5 and 47.0° for DB7. Each CrystalPredictor search covered $Z' = 1$ structures in 14 of the most common space groups ($P1$, $P\bar{1}$, $P2_1$, $P2_1/c$, $P2_12_12$, $P2_12_12_1$, $Pna2_1$, $Pca2_1$, $Pbca$, $Pbcn$, $C2/c$, Cc, $C2$, and $P2_1/m$), generating 1 150 000 plausible crystal structures for B5 and 2 000 000 for DB7. The intermolecular electrostatic interactions

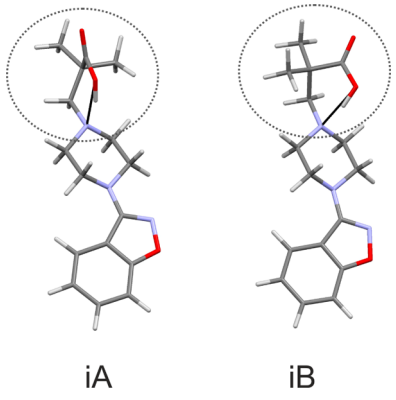

Figure 2. Minimum energy of conformations of B5 with an intramolecular hydrogen bond ($\phi_4 = 0°$) within the iA and iB search regions. The conformations of the acid−piperazine fragments in Figure S5 (Supporting Information) are equal in energy, but the addition of the benzoisoxazole fragment leads to the minimum in the iB region being ~1 kJ mol^{-1} more stable. For DB7, the corresponding minima with the dibenzoxazepine fragment differ by ~3.7 kJ mol^{-1}, with iA being more stable (both PBE0/6-31G(d,p) isolated molecule estimates).

Table 1. Crystallographic Data for B5 Form I and DB7 Forms I and II

phase designator	B5 Form I	DB7 Form I	DB7 Form II
empirical formula	$C_{16}H_{21}N_3O_3$	$C_{22}H_{25}N_3O_3$	$C_{22}H_{25}N_3O_3$
formula weight	303.36	379.45	379.45
temperature/K	100(2)	100(2)	100(2)
wavelength/Å	1.54178	1.54178	1.54178
crystal size/mm	0.20 × 0.10 × 0.05	0.20 × 0.05 × 0.05	0.10 × 0.10 × 0.05
crystal system	monoclinic	triclinic	triclinic
space group	$P2_1/n$	$P\bar{1}$	$P\bar{1}$
a/Å	14.0905(3)	9.3970(3)	9.2754(4)
b/Å	6.2506(1)	10.8925(3)	10.0504(5)
c/Å	17.0170(3)	11.0095(4)	11.8580(6)
α/°	90	65.728(2)	106.010(4)
β/°	91.321(1)	67.321(2)	108.236(3)
γ/°	90	77.584(2)	99.895(3)
volume/Å^3	1498.36(5)	945.71(5)	967.99(8)
Z	4	2	2
density (calculated)/ g cm^{-3}	1.345	1.333	1.303
theta range for data collection/°	4.03−64.91	4.46−65.13	4.77−64.94
index ranges	$-15 \le h \le 16$	$-11 \le k \le 11$	$-10 \le h \le 10$
	$-6 \le k \le 7$	$-12 \le k \le 12$	$-11 \le h \le 11$
	$-16 \le l \le 19$	$-11 \le l \le 12$	$-13 \le l \le 13$
no. of measured, independent and observed [$I > 2\sigma(I)$] reflections	8498/2357/2061	6835/2812/2282	9170/3130/2529
refinement method		full-matrix least-squares on F2	
data/parameters/restraints	2357/206/1	2812/260/1	3130/259/0
goodness-of-fit	1.10 (on F2)	1.05 (on F2)	1.03 (on F2)
final R indices [$I > 2\sigma(I)$]	R_1 = 0.0402	R_1 = 0.0438	R_1 = 0.0392
	$wR2$ = 0.1061	wR_2 = 0.1128	wR_2 = 0.1049
R indices (all data)	R_1 = 0.0454	R_1 = 0.0537	R_1 = 0.0490
	wR_2 = 0.1103	wR_2 = 0.1212	wR_2 = 0.1115
largest diff peak and hole	0.16 and −0.18 e·Å^{-3}	0.24 and −0.25 e·Å^{-3}	0.22 and −0.23 e·Å^{-3}

were initially calculated from atomic charges, but in a subsequent refinement of the CrystalPredictor structures using the DMAflexQuick[28] and DMACRYS[29] algorithms, they were calculated from distributed multipoles[30] derived from analysis of the PBE0/6-31G(d,p) molecular wave function. All other intermolecular energy terms are represented by the FIT empirical exp-6 repulsion-dispersion potential.[29,31] The more stable crystal structures were then refined allowing all of the conformational degrees of freedom depicted in Figure 1, the cell parameters and the molecular positions and orientations to be optimized using the CrystalOptimizer database method,[27] which efficiently uses the calculated ΔE_{intra} and distributed multipoles from the many PBE0/6-31G(d,p) molecular wave function calculations.

Polarization of the molecular charge density within the crystal was investigated by using the polarizable continuum model (PCM)[32] as implemented in Gaussian03. The PCM lattice energies were calculated from the conformational energy and distributed multipoles calculated at the PBE0/6-31G (d,p) level, in a polarizable continuum with $\varepsilon = 3$ (a value typical for organic crystals[32−34]), and the same FIT repulsion-dispersion potential.[29,31] Furthermore, Helmholtz free energies[35] derived from the elastic constants[36] and $k = 0$ phonons[37] calculated in the rigid-body harmonic approximation were estimated for the most stable structures (~200 for each molecule) at 298 K. This approximate Helmholtz free energy surface calculated using the polarizable continuum model to approximate the induction contribution is referred to as the "Crystal Energy" and is reported in section 3.3, with the relative energies for selected structures at the intermediate stages given in section 3.4.3.

More computationally demanding calculations based on different models for the lattice energy were used to further investigate the sensitivity of the crystal energies to the theoretical method. PIXEL calculations[38−40] estimate the repulsive (E_R), dispersion (E_D), electrostatic (Coulombic, E_C), and polarization (also called induction, E_P) contributions to the intermolecular lattice energy, and the contributions from individual pairs of molecules within a crystal are estimated from the charge density for the crystal constructed from the MP2/6-31G(d,p) ab initio charge density of the isolated molecule. Periodic electronic structure calculations were also carried out with the CASTEP plane wave code[41] using the Perdew−Burke−Ernzerhof (PBE) generalized gradient approximation (GGA) exchange-correlation density functional[42] and ultrasoft pseudopotentials,[43] with the addition of a semiempirical dispersion correction (Tkatchenko and Scheffler,[44] TS). To see the effect of changing the dispersion correction, additional single point calculations, using the DFT-TS optimized structures with the addition of the Grimme06 (G06)[45] dispersion correction instead, were performed.

The computationally generated low energy structures were compared using the Crystal Packing Similarity Module in Mercury[46] to determine the root-mean-square deviation of the non-hydrogen atoms in a cluster of n molecules ($rmsd_n$) and the *XPac* program to examine the supramolecular constructs (SCs).[47]

2.2. Materials and Solid Form Screening Experiments. B5 Form I (purity 99.9%) and DB7 Form II (purity 99.6%) were obtained from Lilly Research Laboratories.

The solvent crystallization screens of the two compounds encompassed evaporative crystallization at different temperatures (5, 25, and 50 °C), cooling crystallization (varying the cooling rate), crystallization by standard and reverse antisolvent addition, crystallization by vapor diffusion, crystallization by pH swing using the B5 hydrochloride and DB7 phosphate salts, slurry equilibration, and cross seeding. Over 30 solvents and mixtures thereof, purchased from different suppliers, were used. All solvents used for crystallization screening were reagent grade (99+% purity). Furthermore, hot-stage microscopic investigations and differential scanning calorimetry thermocycling were attempted. In total, more than 300 crystallization experiments were performed per compound in the tailored screens whose crystallization conditions and outcomes are reported in the Supporting Information, section 8 (B5) and section 11 (DB7).

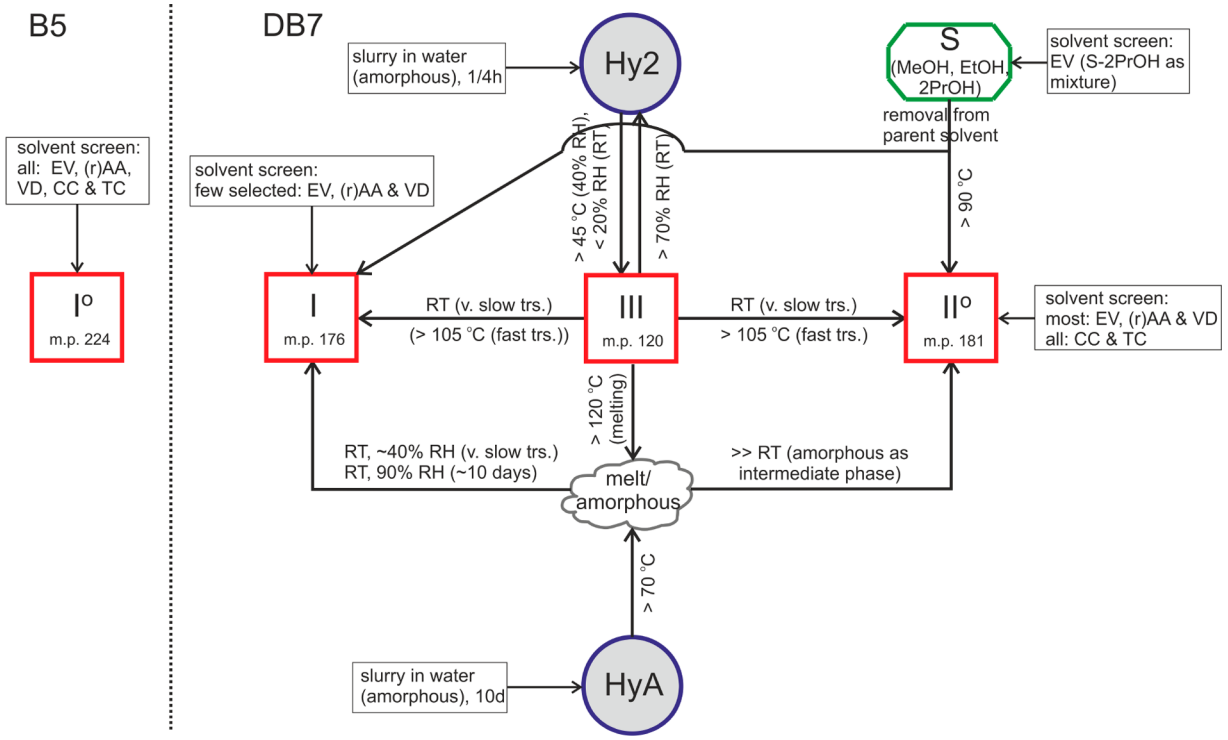

Figure 3. Preparation and transition pathways of the B5 and DB7 solid forms at different temperatures and relative humidities (RH). I, II, and III – anhydrous forms, Hy2 – dihydrate, HyA – hydrate A, S – isostructural solvates from methanol, ethanol, and 2-propanol. Superscript "°" indicates the thermodynamically stable anhydrate form. EV – solvent evaporation, (r)AA – (reverse) antisolvent addition, VD – vapor diffusion, CC – cooling crystallization and TC – temperature cycling experiments.

The anhydrate polymorphs of DB7 were named in consecutive order of appearance, that is, first polymorph Form I, second Form II, etc. Scaling up the screening results led to the following methods for the best phase pure samples used in the subsequent characterization. DB7 Form I was prepared by dissolving 1 g of DB7 in 65 mL of anisole at 90 °C. To complete dissolution, 2 mL of tetrahydrofuran was added. The solution was filtered, cooled to 5 °C, and seeded with Form I seeds (which had been prepared by fast evaporation of DB7 from methyl-*t*-butyl-ether at 50 °C). Heptane (75 mL) chilled to 5 °C was dripped in slowly until precipitation began. The solid product was isolated by vacuum filtration and air-dried at room temperature (RT). DB7 Form II was prepared by dissolving 200 mg of DB7 in 25 mL of methyl isobutyl ketone with light heating. The solution was cooled to RT and seeded with Form II (which had been prepared by slow evaporation of DB7 from ethyl acetate at 5 °C). The solid product was isolated by vacuum filtration and air-dried at RT. DB7 Form III was produced by dehydrating the dihydrate (Hy2) in a 0% relative humidity (RH) (P_2O_5) chamber at RT overnight. Hy2 (280 mg) was prepared by dissolving amorphous DB7 (prepared by rotovapping a dichloromethane solution of the compound) with stirring in 10 mL of water at RT. Within 15 min, a thick white slurry had formed. The solid product was isolated by vacuum filtration and dried initially in a 75% RH chamber and then at ambient RH.

In contrast, the vast majority of the crystallization experiments on B5 gave the same phase-pure neat Form I (Supporting Information section 8). Single crystals were grown by slow evaporation of an acetone solution of B5.

2.3. Single Crystal X-ray Diffractometry. Single crystal X-ray diffraction data for B5 Form I and DB7 Forms I and II were collected using a Cu Kα radiation source (λ = 1.54178 Å) and a Bruker D8-based 3-circle geometry diffractometer equipped with a SMART APEX II 6000 CCD area detector. Cell refinement and data reduction were accomplished using the SAINT software program.[48] The structures were solved by direct methods using the program package WinGX[49] (SIR2004[50] and SHELXL97[51]). Non-hydrogen atoms were refined anisotropically. All hydrogen atoms bonded to carbon atoms were generated by a riding model on idealized geometries with U_{iso}(H) = 1.5U_{eq}(C) for $-CH_3$ groups and U_{iso}(H) = 1.2U_{eq}(C) for all other hydrogen atoms. The polar hydrogens were identified from the difference map and refined isotropically, with the exception of H1 in B5 Form I and DB7 Form I, where the positions were refined with a constrained O–H bond distance. For further details, see Table 1.

2.4. Thermal Analysis. Differential scanning calorimetry (DSC) was conducted using a TA Q1000 DSC. Samples were equilibrated at 22 °C in hermetically sealed aluminum pans and heated to 180–250 °C at 1, 5, 10, or 50 °C min^{-1} with a 50 mL min^{-1} nitrogen purge. The temperature and heat flow were calibrated against indium melting. The stated errors on the given temperatures (extrapolated transition onset temperatures) and enthalpy values are 95% confidence intervals (minimum three measurements).

2.5. Determination of Solubility. In an attempt to quantitatively measure the free energy difference between DB7 Forms I and II as a function of temperature, kinetic solubility measurements were made for the two polymorphs in methyl isobutyl ketone (MIBK) over a range of temperatures using Crystal16 parallel reactors.

2.6. Solid-State NMR Spectroscopy. Cross-polarization/magic angle spinning (CP/MAS) NMR (SSNMR) spectra were obtained on a Bruker Avance III 400 wide-bore NMR spectrometer operating at ^{1}H, ^{13}C, and ^{15}N frequencies of 400.131, 100.623, and 40.546 MHz, respectively, and using Bruker 4 mm triple and double resonance probes. The MAS rate was set to 10 kHz ± 2 Hz using a Bruker MAS-II controller. ^{1}H decoupling was achieved using the SPINAL64[52] decoupling sequence at a proton nutation frequency of 100 kHz for ^{13}C and 50 kHz for ^{15}N. Spinning sidebands were suppressed using a five-pulse total sideband suppression (TOSS) sequence.[53] For acquisition of ^{13}C spectra, a 3.4 ms linear RF power ramp (RAMP100 shaped CP pulse) was used for cross-polarization from ^{1}H to ^{13}C.[54] The acquisition time was set to 34 ms and spectra were acquired over a spectral width of 30 kHz with a recycle delay of 5 s (B5) or 7 s (DB7). The ^{13}C chemical shifts were externally referenced (±0.05 ppm) to the proton-decoupled ^{13}C peak of neat (liquid) tetramethylsilane via the high-field resonance of adamantane (δ = 29.5

dx.doi.org/10.1021/cg500185h | Cryst. Growth Des. 2014, 14, 2056–2072

ppm). ^{15}N CP/MAS NMR acquisition parameters were as follows: 90° proton RF pulse width 2.9 μs, contact time 0.5 (short) or 3.0 (normal) ms, pulse repetition time 60 s, MAS frequency 10 kHz, spectral width 22 kHz, and acquisition time 46 ms. ^{15}N chemical shifts were externally referenced to liquid nitromethane via the ^{15}N peak of α-glycine (δ = −349.5 ppm). Nonquaternary suppression experiments used to remove signals of rigid methine and methylene carbons were conducted using a 50 μs preacquisition delay. Unless specified otherwise, the sample temperature was regulated to 25 °C to minimize frictional heating caused by sample spinning. Low-temperature MAS experiments were conducted using a Bruker BCU-Xtreme temperature controller.

3. RESULTS

3.1. Crystallization Results – The Solid Form Diversity of B5 and DB7. The experimental screen for solid forms resulted in one anhydrate form for B5 (Supporting Information section 8). However, some additional XRPD peaks from products of selected crystallization experiments indicated the possibility of one or more transient phases, present as minor impurities (Tables S13 and S18 of the Supporting Information).

The possibility of using an amorphous DB7 phase, which was considerably more soluble than the DB7 crystalline forms, gave more options in its solid form screen, in terms of vapor diffusion onto solids and slurry crystallizations (Table S26 of the Supporting Information). Three anhydrous forms, two hydrates (a stoichiometric dihydrate (Hy2), and a hydrate (HyA) containing 1.25−1.95 mol of water per mole DB7), three isostructural solvates from methanol (S_{MeOH}), ethanol (S_{EtOH}), and 2-propanol ($S_{2\text{-}PrOH}$), and the amorphous phase emerged from the DB7 solid form screen. Desolvation studies allowed us to further expand the diversity in solid form screen space for DB7, providing the only route to Form III.

Samples of the neat forms suitable for structural characterization by single crystal X-ray diffraction could be obtained for B5 Form I and DB7 Forms I and II, but not Form III, the dehydration product of DB7 Hy2. The work to propose a structural model for Form III is presented in section 3.3.2. SSNMR (section 12.4 of the Supporting Information) shows that the piperazine N3 of DB7 is protonated in the two hydrates, in contrast to the anhydrate forms. A follow-up investigation[55] of the zwitterionic hydrates (c.f. piroxicam,[56] norfloxacin[57]) and their transformations shows how the interactions of DB7 with water complicate the solid-state behavior of DB7.

A summary of the solid forms of B5 and DB7 and their conversion pathways is given in Figure 3.

3.2. Crystal Structures. *3.2.1. B5: Form I.* B5 crystallizes in the monoclinic space group $P2_1/n$, with Z' = 1. The B5 molecule adopts a conformation with the carboxylic acid forming an intramolecular hydrogen bond with the piperazine nitrogen N3, which is similar to the most stable conformation of the isolated molecule, with a rmsd$_1$ of 0.28 Å with conformation iA (Figure 2). Layers of B5 molecules are formed by translation of B5 along the *a* and *b* axes. Adjacent layers are either related by inversion, where the N2 piperazine nitrogen is involved in a weak C−H···N intermolecular interaction forming close packed centrosymmetric B5 dimers or by 2_1 symmetry (Figure 4).

3.2.2. DB7: Forms I and II. DB7 crystallizes in the triclinic space group $P\bar{1}$ with Z' = 1 in both Forms I and II, but the dimethylpropanoic acid side chain of the DB7 molecule adopts distinct conformations in the two anhydrate polymorphs

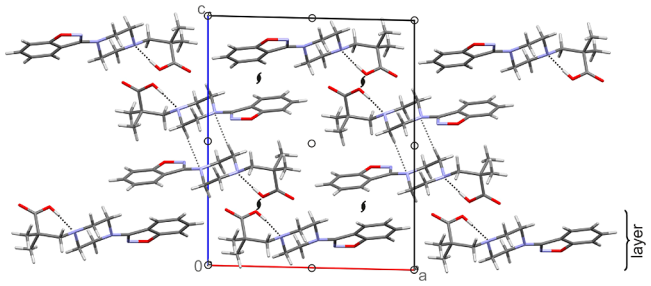

Figure 4. Packing diagram of B5 viewed along the *b* axis. The symmetry elements relating the adjacent B5 layers are shown.

(Figure 5). Both structures are quite close to local minima (ϕ_4 = 180°) in conformational energy of the isolated molecule:

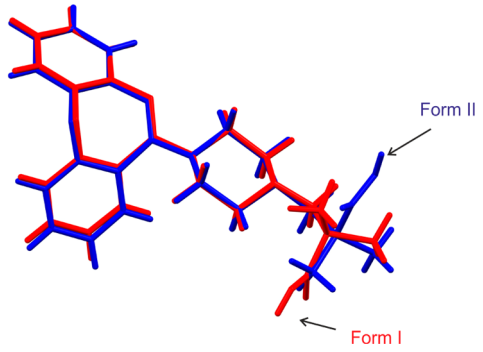

Figure 5. Overlay of DB7 conformations in experimentally observed Forms I (red) and II (blue).

Form I being very close (rmsd$_1$ = 0.15 Å), and Form II (rmsd$_1$ = 0.60 Å) differing from a local minimum structure mainly in the orientation of the carboxylic acid group (ϕ_3). Both DB7 crystal structures have a single, strong intermolecular hydrogen bonding interaction, though to different acceptors, in contrast to the intramolecular hydrogen bond in B5. In DB7 Form I, the O3−H···N1 interaction between the carboxylic acid and the oxepine N links DB7 molecules into chains which propagate along the *a* direction (Figure 6b). In DB7 Form II, the O3−H···N3 interaction between the carboxylic acid and the piperazine N links DB7 molecules into centrosymmetrically related dimers (Figure 6d). In each of the two structures, the DB7 molecules form layers involving the strong O3−H···N hydrogen bonds and C−H···π and π···π interactions to the dibenzoxepinyl ring (Figure 6b,d). Adjacent layers are related by inversion (Figure 6a,c).

3.3. Crystal Energy Landscapes. The most stable calculated structures on the crystal energy landscapes of both B5 (Figure 7a) and DB7 (Figure 7b) correspond to the only (B5, Form I) and most stable (DB7, Form II) experimental structures, respectively. The second structurally characterized DB7 anhydrate, Form I, is found as a higher energy structure but is one of the densest generated. Thus, the crystal energy landscapes are sufficiently realistic to reproduce the known crystal structures well (Figure 8) and make it worthwhile to examine the alternative plausible crystal packings of B5 and DB7 (Figure 7) over a range of low energy and high density structures. The energy gap between the global minimum and the second lowest energy structure is bigger for B5 than DB7 (1.4 kJ mol^{-1} vs 0.2 kJ mol^{-1}), suggestive of a more complex

dx.doi.org/10.1021/cg500185h | Cryst. Growth Des. 2014, 14, 2056−2072

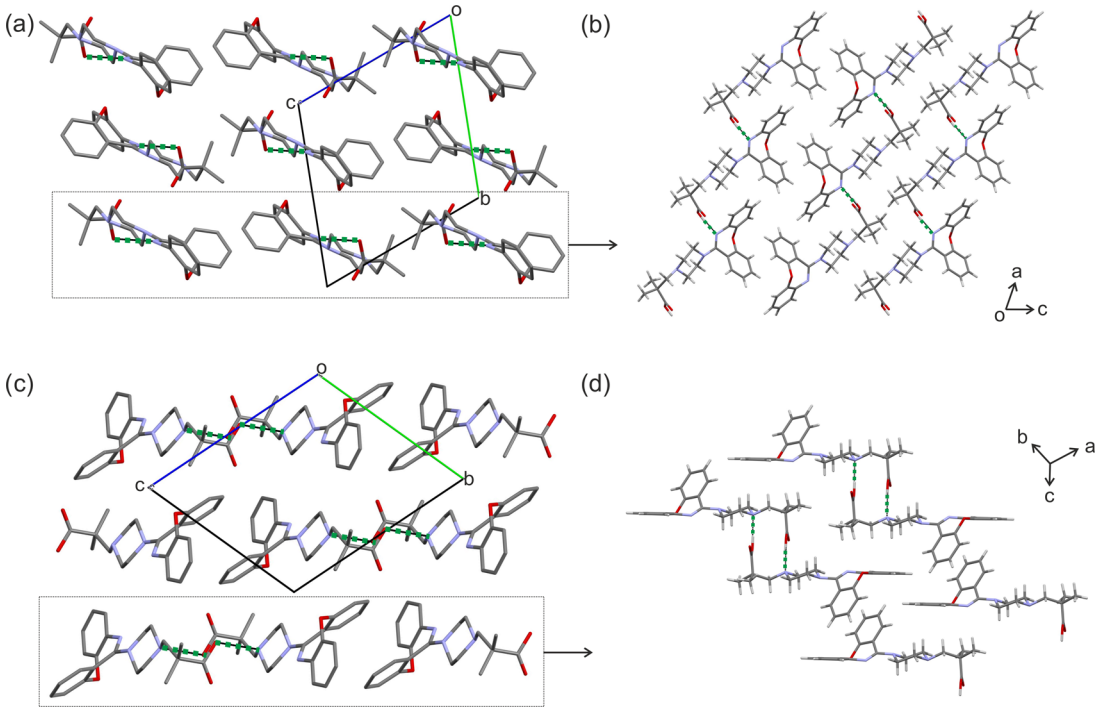

Figure 6. Packing and hydrogen bonding motifs present in DB7 Forms I (a, b) and II (c, d). Hydrogen bonds shown as green dotted lines; hydrogen atoms were omitted in (a) and (c) for clarity.

solid-state for DB7, although these energy gaps are smaller than the uncertainty in our calculations.

The two crystal energy landscapes differ substantially in packing efficiency, with the low energy B5 structures generally falling in the packing index range of 70−74% and the lowest energy DB7 structures being in the 66−70% range. Hence, while the low energy structures of both molecules are within the expected range of packing coefficients for organic molecules, the B5 structures are at the high end and DB7 at the low end of the plausible density spectrum. The calculations thus show that the sterically more demanding dibenzoxepinyl substituent of DB7 cannot pack as efficiently as the planar benzoisoxazole in B5. The packing of the two piperazinyl substituted ring systems is contrasted in section 3.3.1c.

Although a wide range of conformations are low in energy for B5 and DB7 in isolation (section 1 of the Supporting Information) and so were considered in the search, only a limited number of distinct conformers are able to pack in the low energy minima on the crystal energy landscape (Figure 7, section 3.3.1a). The different carboxylic acid conformations favor intermolecular hydrogen bonding as in DB7 Forms I and II and intramolecular hydrogen bonding as in B5. Although counterintuitive, the majority of the calculated low energy B5 structures contain the intramolecular hydrogen bond, while most of the low energy DB7 structures are intermolecularly hydrogen bonded, many involving $R_2^2(12)$ dimers hydrogen bonding the carboxylic acid to the piperazine N3. The hydrogen bonding diversity is analyzed in more depth in section 3.3.1b.

Thus, the crystal energy landscapes show that thermodynamic advantage accounts for the different hydrogen bonding, conformations, and crystal packing observed in the most stable forms of B5 and DB7. Their further use as a complement to solid form screening is to ascertain whether there could be other structures that are likely to be polymorphs and thus see whether the experimental screening appears to have yielded the practically important polymorphs. The appearance of polymorphs reflects the balance between kinetic and thermodynamic effects, and even in the case of B5, the energy preference for the known form is too small to confidently predict monomorphism. Whether the alternative structures are likely to be polymorphs depends on the structural relationships between the hypothetical low energy structures and the known polymorphs,[58,59] which might indicate whether it is likely that they could nucleate separately and exist as distinct free energy minima at finite temperatures. Hence, the next stage is to compare and contrast the more favorable structures labeled in Figure 7 and establish which hypothetical structures warrant careful consideration as potential polymorphs. This analysis is used to propose a structure for DB7 Form III (section 3.3.2). The experimental information on the relative stability of polymorphs is contrasted with the analysis of the sensitivity of the relative energies to the computational model used (section 3.4.3; Table S3 of the Supporting Information).

3.3.1. Structural Diversity on the Crystal Energy Landscapes. (a). Conformational Diversity. Despite the range of conformations covered in the searches, it is notable that only six conformations (nine if the position of the carboxylic acid proton is taken into account) are found among the lowest energy and most densely packed structures for both molecules, and these differ according to the aromatic substituent. For B5, only four conformations (ignoring proton positions) are able to pack (very) densely (Figure 9). The two intramolecularly hydrogen bonded conformers iA and iB found in the majority of the low energy structures are very close to the conformational minima in Figure 2, with rmsd_1 values of less than 0.5 Å and ΔE_{intra} of less than 10 kJ mol^{-1}. The other conformations seen in the low energy B5 structures are intermolecularly hydrogen bonded structures (eA and eD, Figure 9).

dx.doi.org/10.1021/cg500185h | *Cryst. Growth Des.* 2014, 14, 2056−2072

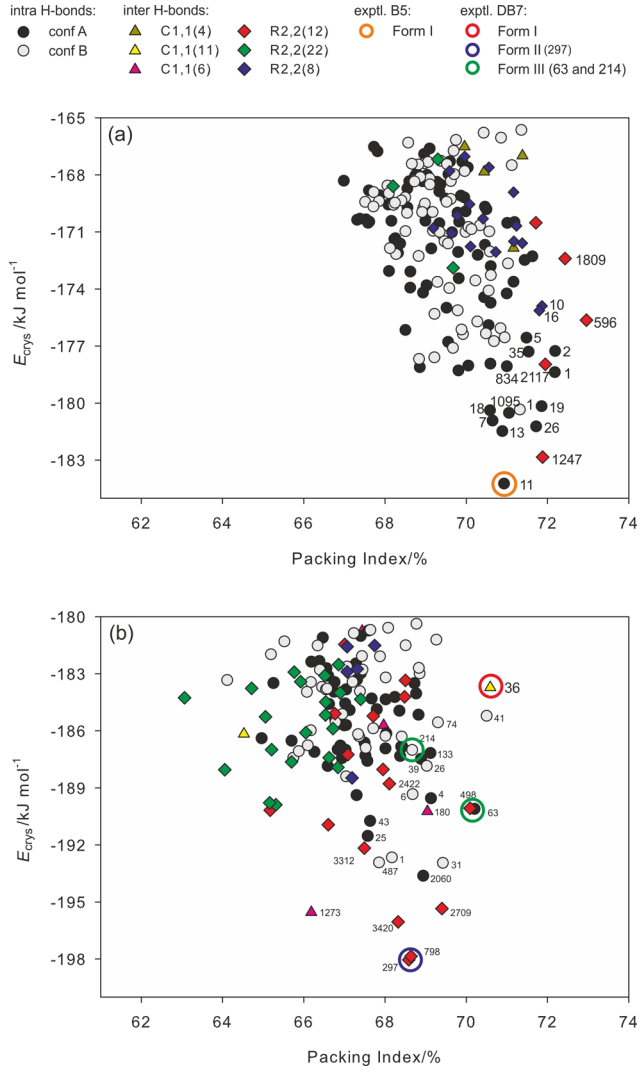

Figure 7. Lowest crystal energy structures for (a) B5 and (b) DB7 generated in CSP searches (PCM + FE results), with the experimental structures encircled. Structures are classified according to hydrogen bonding graph set motifs. The structures used in the analysis and defined in Tables S4 and S5 of the Supporting Information are labeled by their rank on generation by CrystalPredictor and in the text are also labeled by conformation; for example, B5-iA11 corresponds to the only observed B5 structure. The structures in .res format are available from the authors on request.

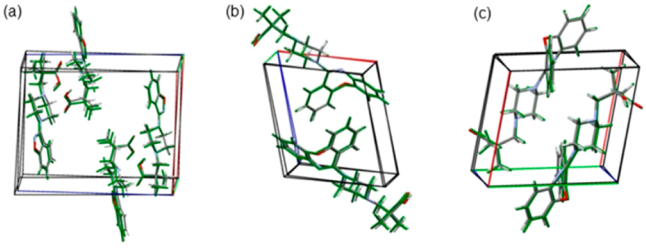

Figure 8. Overlay of the experimental (colored by element) and computed crystal structures (green) of (a) B5 Form I, $rmsd_{15}$ = 0.32 Å, (b) DB7 Form I, $rmsd_{15}$ = 0.22 Å, and (c) DB7 Form II, $rmsd_{15}$ = 0.25 Å.

Five distinct conformations can be found among the most stable and most dense calculated DB7 structures (Figures 7b and 9), three of which are similar to the four B5 conformations.

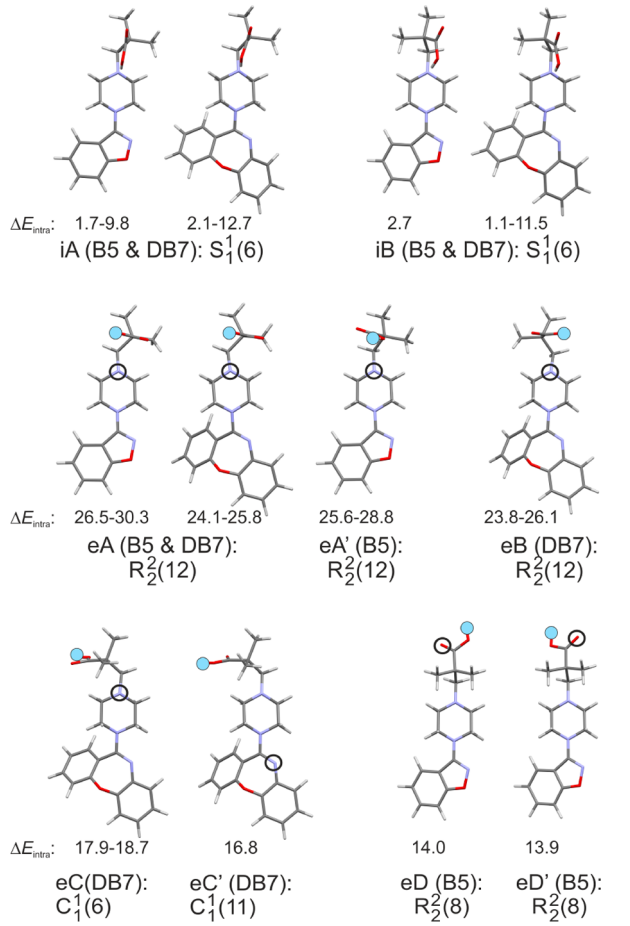

Figure 9. B5 and DB7 conformations and graph-set motifs observed among the most favorable (energy and density, labeled in Figure 7) calculated structures. i – intramolecularly hydrogen bonded, e – intermolecularly hydrogen bonded, conformations marked with (′) differ only by a 180° rotation of COOH. The hydrogen bond donor (light-blue dot) and acceptor groups (open circle) that are used in the most favorable structures of a given conformation are marked for the intermolecularly hydrogen bonded structures. ΔE_{intra} (kJ mol^{-1}) gives the range of conformational energies with respect to the global conformational B5 or DB7 minimum calculated at PBE0/6-31G(d,p) using PCM (ε = 3).

Thus, only conformers eB and eC are observed exclusively for DB7, with the most stable eB structure being Form II, eC giving a structure with a particularly low energy for its low density, and eC′ giving Form I.

(b). Hydrogen Bonding Motifs. Although both molecules have three nitrogen and three oxygen atoms as potential hydrogen bond acceptors, only the intramolecularly hydrogen bonded (Figure 9) and six intermolecularly hydrogen bonded graph-set motifs (Figure 10) are found in the computer generated structures in Figure 7, and each conformation is associated with a particular hydrogen bond acceptor (Figure 9). The variety of hydrogen bonding motifs is even more restricted within the Z' = 1 structures which are explicitly labeled in Figure 7: intramolecular hydrogen bonds and the $R_2^2(12)$ intermolecular motif can be found for both molecules, and DB7 also has as favorable motifs the observed $C_1^1(11)$ and experimentally unobserved $C_1^1(6)$ chains.

(c). Contrasting Packing of the Benzoisoxazolepiperazinyl/Dibenzoxepinylpiperazinyl Moieties. The program *XPac*[47] was used to compare the different crystal packings of the

dx.doi.org/10.1021/cg500185h | *Cryst. Growth Des.* 2014, 14, 2056–2072

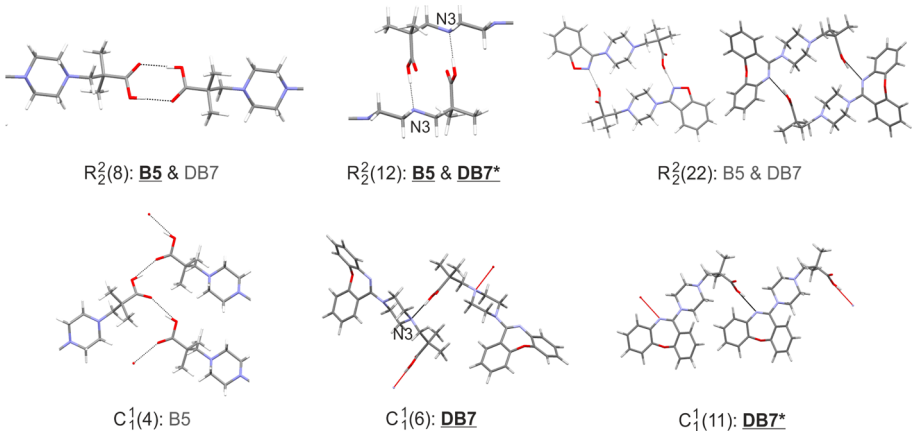

Figure 10. Intermolecular hydrogen bonding motifs observed in the computationally generated B5 and DB7 structures (Figure 7). In bold and underlined are those in labeled structures. Experimentally observed motifs are indicated with an asterisk (*).

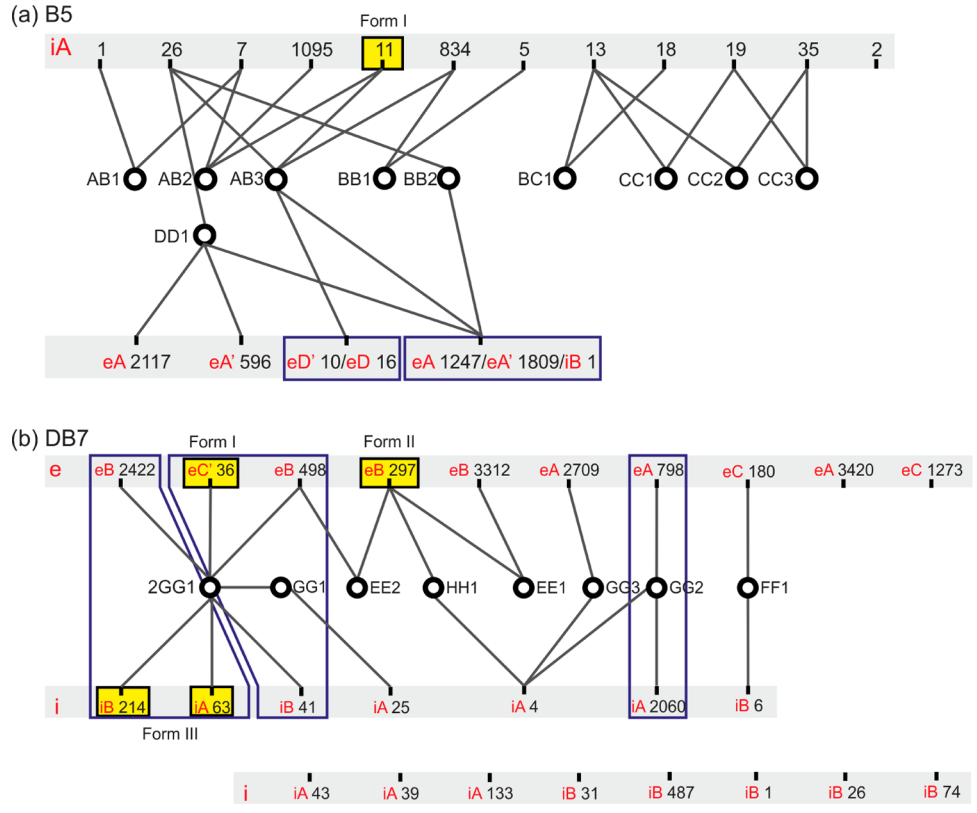

Figure 11. 2D and 3D structural relationships between computationally generated low-energy (a) B5, illustrated in Figure 12, and (b) DB7 structures, illustrated in Figure 13, based on the non-hydrogen atoms of the benzoisoxazolepiperazinyl/dibenzoxepinylpiperazinyl fragments and medium *XPac* cutoff parameters (δ_{ang} = 10°, δ_{tor} and δ_{dhd} = 14°, VdW search radius of 1.5 Å). Numbers correspond to hypothetical crystal structures, with the experimental ones highlighted in yellow. Structures exhibiting 3D similarity are within purple outlined boxes, two-dimensional supramolecular constructs (2D SCs) are the connection points (e.g., AB1), with the letters reflecting similarities. All B5-ABx structures are double layers composed of the same 2D layer AB (Figure 12), and DB7-2GG1 is a double layer of DB7-GG1.

benzoisoxazolepiperazinyl or dibenzoxepinylpiperazinyl (aromatic-piperazinyl hereafter) moiety in the labeled structures (Figure 11) to complement the hydrogen bond analysis. Remarkably, there is 3D similarity between some structures, implying that they have comparable packing of the aromatic-piperazinyl moiety, and yet the different arrangement of the acid group (section 4.1 of the Supporting Information) can change the hydrogen bonding from inter- to intramolecular. However, it is also notable that B5 and DB7 have many structures that have at most a 1D similarity with another structure, including a moderately high energy structure B5-iA2, which has a unique packing arrangement.

For each molecule, it is possible to estimate the intermolecular binding energy within the 2D supramolecular constructs, that is, the average binding energy of the molecules within the layers. The B5-AB2 layer observed in the experimental structure is, according to the PIXEL pairwise estimates (Figure 12), particularly strongly bound. This B5-AB2 layer is also seen in the low energy structures B5-iA7 and B5-iA1095, and so their close relationship to the experimental

dx.doi.org/10.1021/cg500185h | *Cryst. Growth Des.* 2014, 14, 2056−2072

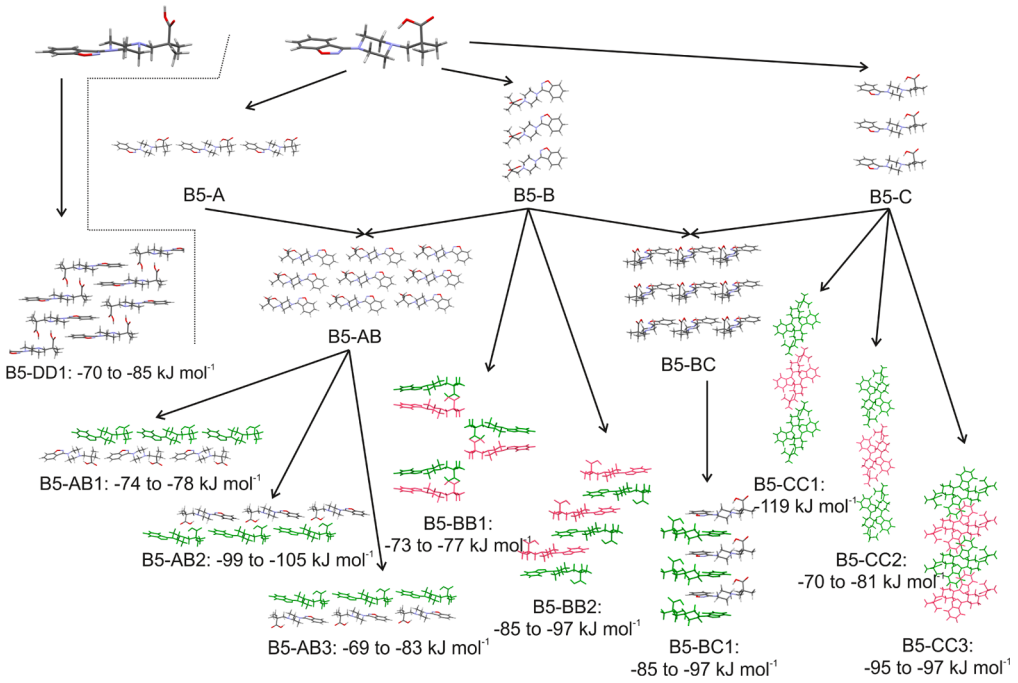

Figure 12. Illustration of the packing similarities of common building blocks (Figure 11a) in labeled structures on the B5 crystal energy landscape (Figure 7a). Note that B5-A, B5-B, and B5-C are 1D SCs, and all others are 2D. The range of energies of each supramolecular construct has been derived from the PIXEL pairwise molecule-molecule energies in Tables S6 and S8 of the Supporting Information.

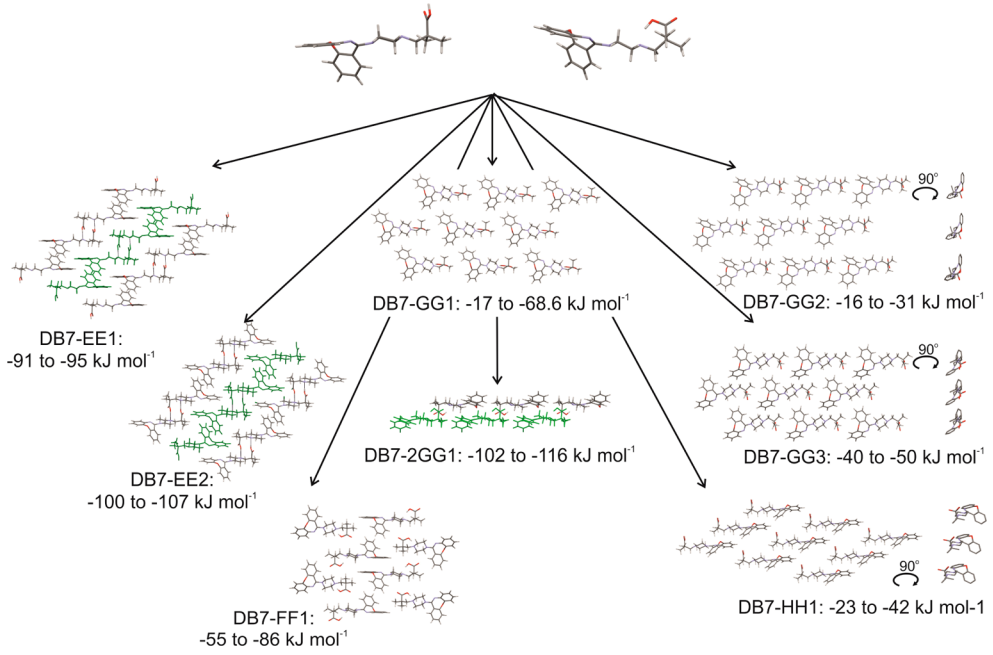

Figure 13. Illustration of the packing similarities of common building blocks (Figure 11b) in the labeled structures on the DB7 crystal energy landscape (Figure 7b). The range of energies of each supramolecular construct has been derived from the PIXEL pairwise molecule-molecule energies in Tables S7 and S9 of the Supporting Information.

form suggests that these structures would have to be trapped in the alternative stackings of this layer, that differ only in weak van der Waals contacts, to be observable polymorphs. The strongest 2D construct is B5-CC1, but this layer does not stack well as the structures in which this is found, B5-iA13 and B5-iA19, have less favorable lattice energies (Table S10 of the Supporting Information) than the experimental structure.

The two strongest 2D constructs of DB7 are present in the experimental forms, DB7-2GG1[60] in Forms I and III (section 3.3.2), and DB7-EE2 in Form II (i.e., the most stable layers lead to stable packings). The relationship between the observed structures is shown by the computer-generated structure DB7-eB498 having 3D packing similarity in the aromatic-piperazinyl moiety to Form I and III, but the Form II eB propanoic acid side chain conformation.

(d). Overall Similarity in Crystal Structures B5 and DB7. The comparison of 19 low energy high density structures on the B5 landscape, and 25 on the DB7 landscape, clearly shows

dx.doi.org/10.1021/cg500185h | Cryst. Growth Des. 2014, 14, 2056−2072

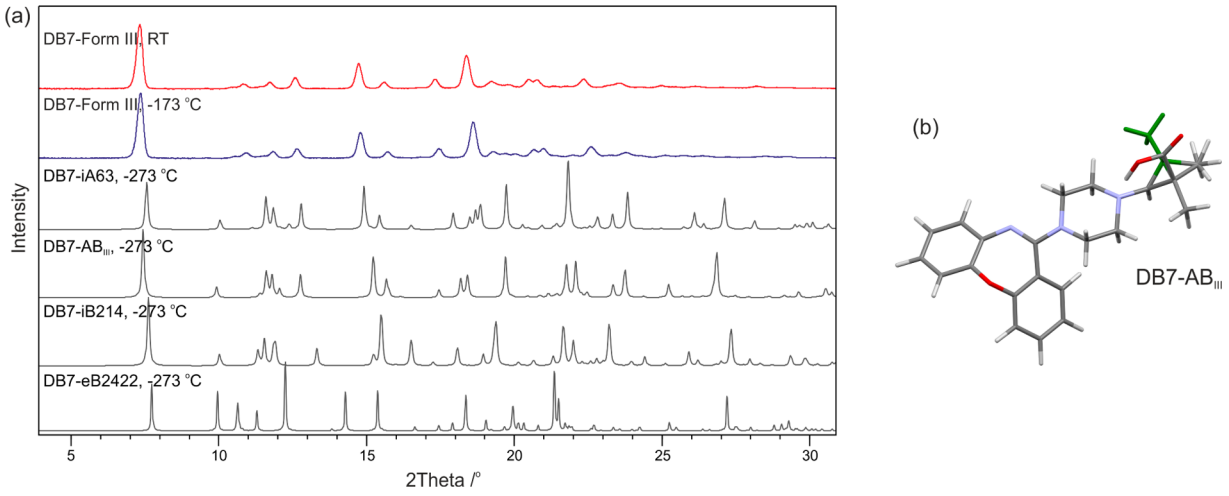

Figure 14. (a) Experimental DB7 Form III powder X-ray diffraction pattern obtained at room temperature and −173 °C (top and second) compared with the closest matching simulated patterns for the computationally generated structures (DB7-iA63, DB7-iB214, and DB7-eB2422) and a hybrid structure DB7-AB$_{III}$ constructed from DB7-iA63 and DB7-iB214. (b) Superimposed asymmetric units of structure DB7-AB$_{III}$, showing the two different conformers proposed to account for site disorder in Form III.

that there is much more structural diversity for DB7 (Figure 11) with many more unique 2D packings of the dibenzoxepinylpiperazinyl fragment of DB7, and many more B5 structures having the same layers of the benzoisoxazole-piperazinyl fragments. The aromatic-piperazinyl packing, conformations (Figure 9), and hydrogen bonding motifs (Figure 10) in the low energy and higher density structures on the crystal energy landscapes (labeled in Figure 7) in relation to the observed structures is important in determining the likelihood that the hypothetical structures could be kinetically trapped as metastable polymorphs, and this is discussed in light of the relative stability of the structures, as determined in 3.4.3. However, first we need to establish the structure of DB7 Form III.

3.3.2. Proposed DB7 Form III Structure(s). Form III is a high energy polymorph, obtained exclusively by dehydrating DB7 Hy2. As a dehydration product, high quality single crystals suitable for X-ray structure analysis could not be obtained. Short contact time solid-state ^{15}N NMR spectroscopy experiments confirmed that DB7 was in the neutral form, and the 1:1 correlation between the number of peaks in the solid-state ^{13}C/^{15}N NMR spectra and the number of carbon/nitrogen atoms in DB7 established that the structure was $Z' = 1$ though there were a couple of notable differences that are discussed later. Therefore, XRPD and the computationally generated crystal energy landscape (Figure 7b) should be capable of deriving the structure of Form III. The experimental Form III diffraction pattern was indexed to a triclinic unit cell (at −173 °C: a = 9.620 Å, b = 10.405 Å, c = 12.206 Å, α = 74.50°, β = 80.74°, γ = 69.13°; at 25 °C: a = 9.510 Å, b = 10.223 Å, c = 12.032 Å, α = 75.01°, β = 81.36°, γ = 68.96°) using the first 20 peaks with DICVOL04 on statistical assessment of systematic absences,[61] as implemented in the DASH structure solution package.[62] This was compared with the simulated XRPD patterns for all of the structures in Figure 7b. Three of the simulated patterns (all $P\bar{1}$, $Z' = 1$ structures) showed a promising match (Figure 14a), with structures DB7-iA63, DB7-iB214, and DB7-eB2422 all having the same (3D) packing of the dibenzoxepinylpiperazinyl fragments. Two structures, DB7-iA63 and DB7-iB214, differ in only the conformation of the dimethylpropanoic acid (Figure 14b). The third structure, DB7-eB2422, differs in conformation and in being an intermolecularly hydrogen bonded structure and was eliminated as a possible structure for Form III by the worse XRPD match (Figure 14) and the absence of any distinct band in the region of intermolecularly hydrogen bonded νN−H) vibrations (above 3020 cm^{-1}).

The decay of diffraction intensity in the experimental Form III XRPD pattern and the fact that the computationally generated structures DB7-iA63 and DB7-iB214 show isostructural packings, differing only in the orientation of the dimethylpropanoic acid group, indicate that the Form III structure may be disordered. This assumption is backed-up by solid-state ^{13}C NMR spectra of DB7 Form III, which consistently show a clear splitting of the peaks for just the methylene and methyl carbons of the dimethylpropanoic acid side-chain (Figure 15). It is also consistent with no peak

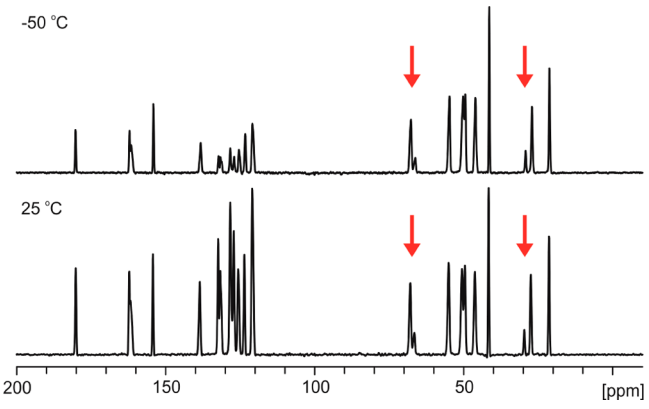

Figure 15. ^{13}C CP/MAS NMR spectra of DB7 Form III at −50 °C (top) and 25 °C (bottom). Peak splitting marked with arrows.

splitting being observed by solid-state ^{15}N NMR spectroscopy (Figure S21, Supporting Information). As shown in Figure 15, aside from the comparatively less intense ^{13}C resonances of the aromatic carbons at −50 °C, there appears to be little difference between the SSNMR spectra collected at 25 and −50 °C, eliminating dynamic disorder as the ratio between the split peak intensities, which is not 50:50, does not change.

dx.doi.org/10.1021/cg500185h | *Cryst. Growth Des.* 2014, 14, 2056−2072

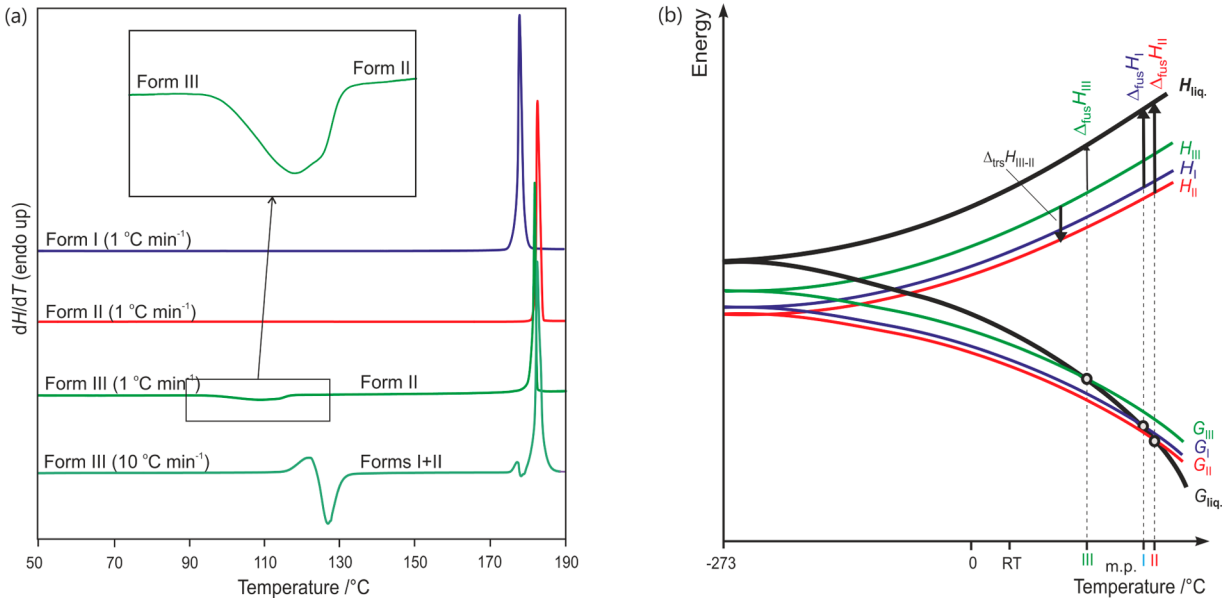

Figure 16. (a) DSC curves of DB7 polymorphs (heating rate 1 or 10 °C min^{-1}). Inset shows the Form III to Form II phase transformation. (b) Semischematic energy/temperature diagram of DB7 polymorphs (I - blue, II - red, and III - green). m.p.: melting point, *G*: Gibbs free energy, *H*: enthalpy, $\Delta_{fus}H$: enthalpy of fusion, $\Delta_{trs}H$: transition enthalpy, liq: liquid phase (melt). The bold vertical arrows mark the experimentally measured enthalpies.

To test the disorder assumption, we constructed a hypothetical P1 $Z' = 2$ structure comprising the two conformers present in DB7-iA63 and DB7-iB214. The structure was lattice energy minimized using both the method used to generate the crystal energy landscape (Figure 7b) and by DFT-D (Table S3 of the Supporting Information). The program PLATON[63] showed that the resulting lattice energy minimum (DB7-AB$_{III}$ hereafter, Figure 14b) can be described as a $P\bar{1}$ $Z' = 1$ structure with a 50% occupancy of the two sites for C18 and C21 (Figure 1). DB7-AB$_{III}$ also gave a powder X-ray diffraction pattern that was a reasonable match to that of Form III (Figure 14), as did the powder patterns with variable occupancy ratios, although there was some variation in the intensity of some peaks (Supporting Information section 6 and Figure S12). The striking similarities between the structures, simulated powder X-ray diffraction patterns and simulated solid-state ^{13}C NMR spectra (Supporting Information section 12.2) of DB7-iA63, DB7-iB214, and DB7-AB$_{III}$ strongly suggest that structures with disorder variation in the conformation would provide a reasonable match to the experimental data on Form III. Thus, a range of disordered structures varying between DB7-iA63, DB7-AB$_{III}$, and DB7-iB214 is consistent with the DB7 Form III being a phase-pure disordered structure.

The ordered structure DB7-iA63 is more stable than DB7-iB214 and DB7-AB$_{III}$, suggesting that more molecules should be in the iA conformation; that is, DB7-iA63 should form the major component if the disorder is being stabilized by configurational entropy.[64] However, as Form III is prepared by dehydrating Hy2, which contains the iB conformation, it is more likely that the disorder arises from an inability of all molecules to change conformation during the dehydration process. Desolvation (dehydration) has often been shown to lead to metastable higher energy forms (e.g., cinacalcet HCl[65]), featuring molecules trapped either in a high energy conformation or high energy packing. It is difficult to estimate the energy barrier to flip from iA to iB within a condensed phase. Hence, the disorder ratio in Form III is likely to depend on the experimental transition conditions. This is consistent with the observation that across all of the Form III materials we have generated to date, we were able to see a range of ^{13}C NMR peak intensity ratios, but we were never able to produce a perfectly ordered Form III sample nor were we able to "flip" the major and minor components—that is, the same conformation was always the major species. Thus, we conclude that DB7 Form III has disorder in the side chain and is based on the structures DB7-iA63 and DB7-iB214, with the ratio of conformations depending on how the sample is prepared.

Forms I and III are closely related (Figure 11); both polymorphs contain the layer DB7-2GG1 but with different conformations of the acid group. For a conversion to occur in the solid-state, the iA and iB molecules in Form III must change conformation so that the intramolecular hydrogen bonds in Form III become intermolecular in Form I. The observation that Form III transforms easily to Form I confirms that the rearrangement of the acid group, despite involving changes in hydrogen bonding, is relatively facile.

There is a considerable difference between metastable Forms I and III and the stable Form II, both in conformation, hydrogen bonding, and the packing of the aromatic-piperazinyl moiety. Thus, the transformations (Figure 3) to the most stable polymorph involve considerable rearrangement (Figure 9) consistent with Form I and III being kinetically stabilized metastable polymorphs.

3.4. Thermodynamic Stability of DB7 Anhydrous Forms. *3.4.1. Thermal Measurements/Semischematic Energy Temperature Diagram.* The three anhydrate polymorphs of DB7 were examined with DSC (Figure 16a). The DSC curves of Forms I and II show only the melting of each of the two forms: melting for Form I occurs at 176.0 ± 0.3 °C (onset temperature) with an enthalpy of fusion of $\Delta_{fus}H_I$ = 43.4 ± 0.3 kJ mol^{-1}, and melting of Form II is observed at 180.9 ± 0.1 °C with an enthalpy of fusion of $\Delta_{fus}H_{II}$ = 48.3 ± 0.2 kJ mol^{-1}. Since Form II melts at a higher temperature and exhibits a higher enthalpy of fusion than Form I, it can be concluded from

dx.doi.org/10.1021/cg500185h | *Cryst. Growth Des.* 2014, 14, 2056−2072

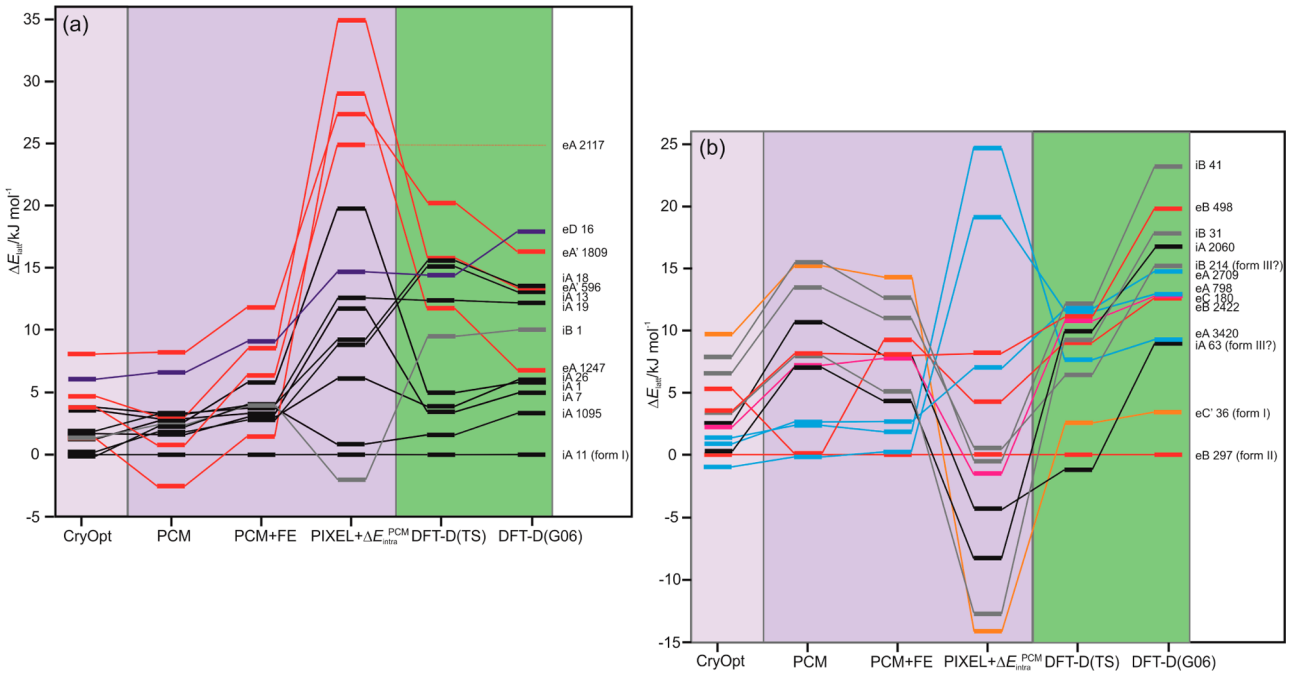

Figure 17. Relative lattice energies of the most stable computationally generated (a) B5 and (b) DB7 structures calculated using different methods: CryOpt − CrystalOptimizer, PCM − isolated molecule relaxed structures with average polarization from the PCM model, PCM + FE − crystal energy using PCM with the addition of rigid-body free energies, PIXEL + ΔE_{intra}^{PCM} − PIXEL U_{inter} energies with the addition of PCM ΔE_{intra}, DFT-D, periodic density functional theory relaxations with dispersion correction (TS or G06). Tie lines have been added to highlight the changes in relative ordering. Structures with same hydrogen bonding motif/conformations (Figures 9 and 10) have the same color. Each background color indicates that the structure was that obtained by optimization by the first method and kept fixed for re-evaluation within the following methods.

the heat of fusion rule[66] that the two forms are monotropically related. Upon slowly heating Form III (heating rate of 1 °C min^{-1}), an exothermic phase transformation to Form II with an onset temperature at 95.9 ± 0.1 °C and an enthalpy of transition ($\Delta_{trs}H_{III-II}$) of −13.3 ± 0.2 kJ mol^{-1} occurs. Traces of Form I may also be present after the solid-state transformation. By applying faster heating rates (>5 °C min^{-1}), the melting point of Form III was observed between 118 and 121 °C, followed by a recrystallization process, the melting of Form I, another recrystallization process, and finally the melting of Form II. The melt of Form III produced by fast heating crystallizes mainly as Form II with some Form I, in marked contrast to the difficulty of nucleating Form I or Form II from any melt of Form I or Form II (Figure S19 of the Supporting Information). To test the hypothesis that seed crystals of Form I/II could have been present to induce crystallization with heating, DSC experiments were conducted for Form III spiked with either 3% Form I or Form II. Spiking did not appear to change the outcome. Furthermore, spiking the cooled melt of DB7 with Forms I or II and heating the mixtures did not lead to recrystallization, suggesting that Form III may have templated the crystallization of the more stable polymorphs.

A monotropic stability relationship[66] between Forms I and III and Forms II and III was established by the observation of Form III melting near 120 °C and the lower enthalpy of fusion $\Delta_{fus}H_{III}$ = 35.3 ± 0.4 kJ mol^{-1} (calculated by applying Hess' law: $\Delta_{fus}H_{III} = \Delta_{fus}H_{II} + \Delta_{trs}H_{III-II}$). Hence, the thermodynamic relationship of the three forms of DB7, shown in a semischematic energy temperature diagram (Figure 16b), has no transition points; that is, none of the free energy curves intersect below the melting point. Collectively, the rank order of stability of the DB7 polymorphs at all temperatures (below melting) is Form II > Form I ≫ Form III. A phase pure sample of Form I, kept in a glass vial under ambient conditions, did not transform to the stable Form II within the 18 months of the investigation, indicating that the kinetic stability of Form I is high. In contrast, samples of Form III, kept under the same conditions as Form I, completely transformed to mixtures of Forms I and II.

3.4.2. Solubility Experiments. Form I was confirmed to be more soluble (less stable) than Form II between 30 and 60 °C in methyl isobutyl ketone, and kinetic solubility data plotted in van't Hoff form, allowing for extrapolation to higher and lower temperatures, showed no signs of convergence, let alone crossover (section 12.3 of the Supporting Information). These data support the DSC interpretation of a monotropic stability relationship between Forms I and II, with Form II being thermodynamically more stable at all temperatures. More quantitative stability differences could in principle be obtained from equilibrium solubility measurements,[12] but the equilibrium solubility of Form I could not be determined, as all but one measurement in ethanol, methyl ethyl ketone, acetonitrile, and methyl isobutyl ketone at 20, 30, 40, and 50 °C showed at least partial conversion of Form I to Form II. These results nonetheless confirm that Form II is the thermodynamically stable polymorph, at least in the temperature range of greatest importance in pharmaceutical development.

3.4.3. Relative Lattice Energy Differences. The experimental DSC data suggest that the lattice energies relative to Form II of DB7 should be approximately 4.9 ± 0.8 kJ mol^{-1} for Form I and 13.3 ± 0.2 kJ mol^{-1} for Form III, making the common but questionable assumption that the heat capacities and zero-point energies are the same for all polymorphs.[12,67] This, and the relative stability of DB7 Form II and the only known structure of B5 relative to a representative sample of the computer

dx.doi.org/10.1021/cg500185h | *Cryst. Growth Des.* 2014, 14, 2056−2072

generated structures, can be used to assess different methods of estimating the crystal energies (Figure 17 and section 5 of the Supporting Information).

Assuming that the conformational energy penalty and molecular charge distribution were the same as in the isolated molecule gives the CryOpt structures in Figure 17 in which the conformation was allowed to change due to the packing forces. Approximating the crystal environment by a polarizable continuum[33] in the calculation of ΔE_{intra} and the distributed multipoles and reoptimizing the lattice with the molecule held rigid (Figure 7, PCM in Figure 17) stabilizes most of the intermolecularly hydrogen bonded crystal structures (eA, eB, etc.) relative to structures where the hydrogen bond is intramolecular (iA or iB). However, using the PIXEL estimate of the intermolecular lattice energy with the polarization, as well as all other terms estimated by integration over the isolated molecule ab initio charge density and the PCM intramolecular energy penalty, markedly destabilizes the intermolecularly hydrogen bonded structures for B5. Although the PIXEL model evaluates the intermolecular energy, particularly the polarization, in a more crystal and molecule specific way, the inability to optimize the crystal structures with this energy model will affect the relative energies as they are very sensitive to the crystal structure.[68] Complete optimization of these crystal structures with a periodic electronic structure method (DFT-D(TS)) leads to significant rerankings relative to the lattice energy methods based on molecular electron density calculations, expanding the energy range particularly for B5. These periodic methods should provide a better optimization of the molecular conformation and crystal packing and treat all inter- and intramolecular forces in the same way. Furthermore, proton migration from the neutral to the zwitterionic state may be possible during the optimization, although it only occurred for one hypothetical structure, B5-eA2117 (Table S10, Supporting Information). However, the calculations are extremely expensive, even using a functional that gives a significantly worse description of the molecular charge distribution than was used for the single molecule charge densities. The periodic electronic structure methods require an empirical correction for the dispersion energy, and re-evaluating the periodic ab initio energy with a different dispersion correction (DFT-D(G06)) provides a significant reranking and expansion of the energy range for DB7, changing the most stable structure from a likely component of Form III to the correct structure Form II (Figure 17).

B5 and DB7 are particularly demanding of methods of evaluating the lattice energy because of the range of conformations, types of hydrogen bonding and predominantly dispersion bound close contacts, including many $\pi\cdots\pi$ and C−H$\cdots\pi$ interactions that give a total lattice energy within a small energy window. PIXEL evaluations of the different contributions between pairs of molecules within the crystal structures (Tables S6−S9 of the Supporting Information) show that the dispersion generally is the most important contribution to lattice stability, usually greater than the electrostatic contribution, but often smaller than the combined electrostatic and polarization contributions. For example, pairs of stacked intramolecularly hydrogen bonded B5 molecules have a similar energy from the dispersion interaction to pairs of molecules connected by intermolecular hydrogen bonds.

For both molecules, the $R_2^2(12)$ intermolecular interaction (Figure 10) is the most stable pairwise interaction (ignoring ΔE_{intra}) as it involves both hydrogen bonding and dispersion stabilization. The other intermolecularly hydrogen bonded pairwise interactions are of the same magnitude as pairs of intramolecularly hydrogen bonded molecules (section 5.1 of the Supporting Information), emphasizing that we cannot assume that hydrogen bonding predetermines the crystallization behavior of B5 or DB7.

The DFT-D models were relatively successful in calculating reasonable energy differences between DB7 Forms I and II (+2.61 kJ mol^{-1} and +3.55 kJ mol^{-1} using the TS and G06 dispersion corrections respectively, in comparison to the experimental $\Delta_{trs}H_{II-I}$ = 4.9 ± 0.8 kJ mol^{-1} from the difference of $\Delta_{fus}H$). The other methods gave an unrealistic energy difference of over 10 kJ mol^{-1} (Figure 17).

The relative stability of crystal structures should be determined by the Gibbs free energy, rather than the lattice energy, although the observed monotropic relationship between the polymorphs implies the same ranking. A crude estimate of the differential free energy from the effect of harmonic rigid-molecule motions within the lattice does cause significant reranking (contrast PCM and PCM + FE in Figure 17), showing that the neglect of thermal effects is another uncertainty in the relative energies. Given that the theoretical basis for these methods have different strengths and weaknesses for the different contributions to the crystal energy, we can only conclude that the observed form of B5 and Form II DB7 are the most stable forms (consistent with experiment) within the errors of the currently available computer models.

4. DISCUSSION

4.1. Different Crystallization Behavior of B5 and DB7.

The close structural relationship between B5 and DB7, including the same hydrogen bonding functionality, might have been expected to lead to related solid forms. However, B5 readily crystallizes but in only one structure (Figure 3) with intramolecular hydrogen bonding (Figure 4), whereas DB7 forms three polymorphs, an amorphous form and a variety of hydrates and solvates (Figure 3). The two ordered DB7 polymorphs, I and II, have intermolecular hydrogen bonds, yet Form III appears to have intramolecular hydrogen bonds. The unexpected difference in the hydrogen bonding is explained by the calculations, which suggest that the structures of B5 Form I and DB7 Form II are the most stable (Figure 17) with the difference in substituents affecting the packing efficiency and hence the balance of the dispersion and hydrogen-bonding interactions. The crystal energy landscape of DB7 was used to find structures which gave reasonable matches to the XRPD pattern of Form III and to propose a structure, which is likely to be disordered, helping to characterize this form. Hence, this study has illustrated both of the anticipated uses of a CSP study—confirming that the most stable structure has been found and helping determine the structures of polymorphs by finding which best match powder patterns and SSNMR spectra. However, it has also illustrated the challenge of such applications for molecules such as DB7: the computational energy ranking is not yet sufficiently reliable when the structures are so close in energy, and the disorder resulted in more than one generated structure providing a match to the powder diffraction (Figure 14) and SSNMR data (Figure S24 of the Supporting Information) of Form III.

Experimental screening is not a wholly automated process: the discovery of the metastable forms of DB7 relied in part on the formation of amorphous and solvated forms, which could not be similarly produced for B5 (section 8.9 of the Supporting

Information). Establishing the relationships between the different solid forms of DB7 required tailored experimentation, though this effort was focused by the simultaneous analysis of the experimental data and the crystal energy landscape. Since the calculations only generate structures that are thermodynamically plausible and the barely understood kinetics of crystallization determines which of them may be observed,[58] the crystal energy landscapes can only currently be used to understand the occurrence of metastable polymorphs and to rationalize complex crystallization behavior in conjunction with solid form screening. Thus, it is the complementarity afforded by packing analysis of structures calculated to be thermodynamically plausible[69] and the full elaboration of the experimental solid form landscape that, when conducted simultaneously, allows a comprehensive picture of the crystallization possibilities to emerge.

4.2. Do We Expect to Find More Polymorphs? The analysis of the similarities and differences in the more likely (lower energy) CSP generated structures is an extension of the skills being adopted by scientists in understanding their experimental crystal forms[47,70−72] to larger collections of structures. However, interpreting whether the relationships imply that the unobserved structures may be metastable polymorphs, components of disorder, or could never crystallize needs the experience of this type of study.[58]

Provided that a reasonable packing (within the packing index range ∼65−75%) is achievable, a molecule may be expected to exist in at least one stable crystal structure: realizing potential metastable polymorphs from the crystal energy landscape (Figure 7), on the other hand, will depend on there being a route to selectively form or possibly trap them. For DB7, the conformational energy barriers estimated for an isolated molecule are quite large, in particular, for ϕ_1, ϕ_2, and ϕ_5 (Figure 1), but the PCM calculations suggest that they would be significantly moderated by the environment. Such estimates are challenging as concerted minor adjustments of multiple torsion angles can produce the transformation between conformation iA and iB (Figure 2) more readily than a 180° rotation of the dibenzoxepinyl ring (ϕ_5), which is implausible in a condensed phase. Certainly, the different conformations in the observed forms and their transformations suggest that the barriers to rearrangement of the molecules can be overcome in solution, in the melt and sometimes even in the solid state. This makes it difficult to judge whether the other plausible generated structures could be kinetically trapped as metastable polymorphs.[58] Although the ease of conformational change in dilute solutions will be very similar for both molecules, the kinetics of conformational change may well differ in the supersaturated solutions encountered in the crystallization process. Fast crystallization into the more densely packed B5 structures may restrict conformational rearrangement, whereas the poorer packing and disorder in Form III, which is prepared from Hy2, shows that conformational rearrangement can occur within the condensed phases of DB7.

B5 can close pack with itself remarkably well in the most stable structure, with a conformation very close to the most stable in isolation (Figure 2). This is perhaps surprising for such a complex molecular shape but has also been observed for another model pharmaceutical GSK269984B.[20] Both form only one anhydrous form and crystallize easily in the lowest energy structure. There are other B5 structures that are within the energy range of polymorphism; however, the two that are probably the most thermodynamically competitive, B5-iA1095 and B5-iA7, share the same highly stable 2D construct B5-AB2 with the observed form. The fact that B5-iA11 (Form I) was observed in all crystallization experiments (section 8 of the Supporting Information) implies that B5-iA1095 or B5-iA7 may not be trapped as distinct structures during crystallization. The most thermodynamically plausible potential metastable polymorph of B5 is B5-eA1247, as this has one of the most distinctive packing arrangements, featuring the $R_2^2(12)$ dimer seen in DB7 Form II. Attempts to seed the crystallization of B5 with DB7 Form II did not yield a novel polymorph from solution (Table S27 of the Supporting Information). The fast crystallization kinetics of B5 Form I and the difficulty of avoiding seeding with this form probably account for the observed (or apparent) monomorphism of B5.

In contrast, DB7 has no good way of packing with itself to give a dense structure. By forming intermolecular hydrogen bonds, it can produce stable structures but with a lower packing efficiency than B5. It seems likely that this accounts for the propensity of DB7 to form solvates. The CSP generated structures in Figure 7 do not have voids large enough to accommodate solvent molecules, in contrast to the behavior of the frameworks of inclusion compounds,[73] but this may reflect a low barrier to collapsing to a neat form. Certainly, the crystallization behavior of DB7 (Figure 3) is linked to the formation of solvates/hydrates, though there is no close relationship between the characterized zwitterionic hydrates and the lower energy unobserved structures. This is not surprising, as different proton positions and hence hydrogen bonding directionality usually produce different low energy structures.[8,74,75] Proton positions usually have a major effect on relative energies of otherwise similar structures, though some hydrates provide exceptions leading to disorder.[8,76] The structural diversity on the crystal energy landscape of DB7 may also account for the ease of forming an amorphous phase.[77] The ability to find solvates and use amorphous input material meant that a wider range of crystallization conditions could be explored for DB7 than B5 and led to the discovery of Form III. The diversity of structures means that we cannot exclude even more neat forms being found for DB7, but the relative energy calculations (Figure 17) suggest that these are likely to be as metastable as Forms I and III. We have probably found the most practically important polymorphs because the observed forms feature the most stable layers and diverse packings. Thus, this study is sufficient to provide reassurance that the most stable neat forms of B5 and DB7 are known, and if either were to be progressed in development, further seeking of polymorphs would not appear to be warranted. However, further work on the hydrates of DB7 would be necessary, as described in a forthcoming paper.[55]

4.3. Value of Calculations and Readiness for Use in Solid Form Screening. Solid form screening is an essential step toward ensuring that suitable solid-state forms are incorporated by design into quality drug products. Given this and other recent successes in predicting crystal structures of molecules approaching the complexity of typical modern pharmaceuticals,[10,18−29] CSP appears to be poised to significantly enhance pharmaceutical development by providing a reassurance of having found all practically important polymorphs (i.e., the one to be incorporated in the drug product and those whose formation needs to be avoided by the design of the crystallization process). In this study, the calculation of the crystal energy landscapes and consideration of possible conformations of moderately complex, but

structurally related B5 and DB7, were sufficiently accurate to rule out there being significantly more stable and less soluble undiscovered neat polymorphs, where "significant" is on the scale of the solubility, stability, and conformational difference of ritonavir,[78] at least with respect to $Z' = 1$ structures in the 14 most common space groups. However, the methods currently available were not able to reliably calculate the relative lattice energies of DB7 Forms I−III, let alone their free energy differences. In fact, accurately predicting the stability order of polymorphs of even small organic molecules such as methylparaben[79] at temperatures relevant to drug processing and storage remains a challenge for developing computational methods.[80,81]

A major difficulty with using CSP to augment industrial solid form screening is the computational expense in terms of resources and time currently required to generate a crystal energy landscape. The time that it takes to complete the calculations is typically longer than that allotted during drug development to select a final crystal form and is further increased with the use of different methods of assessing the relative energies, the number of structures that need to be carefully evaluated, and the need to calculate properties, such as SSNMR spectra. All of these factors depend on the energy gaps and range of structures for the specific molecule,[82] which will only be apparent once a reasonable approximation to the crystal energy landscape has been calculated.

The computational cost of our study is consistent with the suggestion[20] that CSP studies would be most obviously worthwhile for compounds in late-stage development, which is well after most solid form landscapes are typically explored experimentally. In this scenario, the value of a calculated crystal energy landscape will not only be to reaffirm that the practically important polymorphs have been found but also to retrospectively rationalize crystallization behaviors, polymorph appearance, solid-state stability, and transformation pathways. For B5 and DB7, the crystal energy landscapes certainly helped to explain at the molecular level the diverse crystallization behavior observed for these two molecules. This type of information is invaluable for attaining process understanding and has surely brought a sense of closure to the solid form survey. However, having a crystal energy landscape available late in development, long after solid form screening is presumed to have delivered the final crystal form, arguably leaves little time to react to it, particularly when more stable packings are calculated. In such cases, the solid form investigations of a compound that is active in development would inevitably be reopened to find them and, if successful, could prompt a switch to a more stable form. Needless to say, late form changes are almost never welcome, requiring crystallization and formulation processes to be reworked and the bioequivalence of the new form to ultimately be demonstrated, all of which invariably add considerable delays to development timelines and increase cost.

We have found that having the crystal energy landscape available during the solid form screening process can be very advantageous, with the combined disciplines helping to clarify the experimental solid form landscape and suggest new experiments and calculations to be explored. For DB7 Form III, a disordered structure based on two closely related packing arrangements on the crystal energy landscape was proposed to account for the peak splitting observed by solid-state ^{13}C NMR spectroscopy (Figure 15) and in so doing rule out the possibility of a concomitantly crystallized fourth polymorphic form being present as a phase impurity. Having a clearly predicted potential polymorph and its structure, on the other hand, may suggest a specific route to find it, such as isomorphic seeding as demonstrated for catemeric carbamazepine form V[83] and phenobarbital polymorphs,[84] or more general approaches, such as crystallization under pressure,[85] to find denser forms. Although the crystal energy landscapes of B5 and DB7 did not suggest a worthwhile target structure, further research in developing such strategies will undoubtedly have industrial application. Given the strong preference to identify and lock in the solid-state form as early as possible in drug development, CSP needs to be applied to drug candidates in real time, that is, concurrently with experimental solid form screening. Thus, better algorithms and advances in computer power will be required to improve the computational speed.

CSP methods have yet to evolve to the point where a full solid form landscape comprising $Z' > 1$ neat forms, solvates, salts, and cocrystals could collectively be entertained, let alone routinely explored for molecules of typical pharmaceutical complexity. Still, with approximately 50% of pharmaceuticals having been reported to exhibit polymorphism,[86] studies like this show how combining experimental and in silico solid form screening to explore the solid form landscape of neat polymorphs alone could help to right-size the experimental search for relevant crystal forms. In cases where there simply are not many competitive polymorphs or the forms appear early or with relatively minimal effort, experimental solid form screening will almost always extend well beyond the point of diminishing returns before the screens are confidently judged as complete. Having assurance from the crystal energy landscape that all practically important polymorphs have been found, experimental screening efforts could be redirected to specifically finding other equally important forms, including hydrates and solvates. With B5 and DB7, however, we are reminded of the danger in reading too much into even a reasonable approximation of the crystal energy landscape early on, as predicted structures may be significantly reranked with different, equally well-justified approximations to the relative energies (Figure 17).[87] The uncertainty in the energy calculations, coupled with the ability to trap kinetic forms, for example, by desolvation, means that experimentally accessible forms could be among the high energy structures in the crystal energy landscape. Such was the case for DB7 Form III. Thus, before we can truly benefit from CSP studies, we need more studies like this one, contrasting the structural relationships of the computed crystal energy landscape with the structures and transformations found with industrial standard screenings, to gain confidence in their interpretation in terms of polymorphs, solvates, and disorder through to amorphous phase formation.

5. CONCLUSIONS

Two closely related piperazinyl-dimethylpropanoic acids, B5 and DB7, differ markedly in their solid form landscape, with only one crystal structure of neutral B5 being found, whereas DB7 formed solvates (hydrates) and an amorphous form which allowed more extensive screening. The structures of B5 Form I and DB7 Forms I and II were solved by single crystal diffraction, and a disordered structure for DB7 Form III was proposed by combining powder diffraction, SSNMR, and structures on the calculated crystal energy landscape. From the complementary use of computational and experimental screening data, it appears that hydrogen bonding is not the dominant driving force for the self-assembly of these molecules, and the

differences in the favorable packing ability of the benzoisoxazolepiperazinyl and dibenzoxepinylpiperazinyl fragments account for the different propensity toward solid forms.

Further developments in our ability to calculate the relative stability of crystal structures of pharmaceutical molecules, such as DB7 and B5, where conformational flexibility and functional group diversity produce a range of favorable structures, are required but are a challenge to computational chemistry modeling. However, CSP methods have advanced to a stage of complementing solid form screening in helping bring together the experimental observations and focus further experimentation by providing a sense of the range of alternative structures that are thermodynamically competitive.

■ ASSOCIATED CONTENT

Supporting Information

Computational model selection and conformational analysis; reproduction of the experimental B5 and DB7 structures by different computational models; structure comparisons; PIXEL energies and enlargements of Figures 12 and 13; DFT-D calculations; modeling of DB7 Form III; solubility data; solid form screens; solid-state characterization: thermal analysis, X-ray diffraction, solid-state NMR, moisture sorption/desorption studies. This information is available free of charge via the Internet at http://pubs.acs.org. Crystallographic information files are also available from the Cambridge Crystallographic Data Center (CCDC) upon request (http://www.ccdc.cam.ac.uk, CCDC deposition nos. 984272 (B5, Form I), 984273 (DB7, Form I), and 984274 (DB7, Form II)).

■ AUTHOR INFORMATION

Corresponding Author

*E-mail: doris.braun@uibk.ac.at. Tel: +43(0)512 507 58653.

Notes

The authors declare no competing financial interest.

■ ACKNOWLEDGMENTS

Profs. Pantelides and Adjiman (Imperial College London) are thanked for use of CrystalPredictor and CrystalOptimizer codes. The authors also thank Ben Diseroad (Lilly) for diffraction datasets, Dr. Sreenivas Lingireddy (Lilly) for capillary diffraction experiments, David Jackson (Lilly) for solid-state NMR experiments, Dr. Jeff Tan (Lilly) for assistance with solid-state NMR chemical shift prediction and Dr. Suk-fai Lau (Lilly) for thermal analysis support. This work was supported by Eli Lilly and Company through the Lilly Research Awards Program (LRAP), and the DFT-D calculations by the Austrian Ministry of Science BMWF as part of the UniInfrastrukturprogramm of the Research Platform Scientific Computing at the University of Innsbruck.

■ REFERENCES

(1) Hilfiker, R. *Polymorphism in the Pharmaceutical Industry*; Wiley-VCH: Weinheim, 2006.
(2) Brittain, H. G. *Polymorphism in Pharmaceutical Solids*; Informa Healthcare: New York, 2009; Vol. *192*.
(3) Storey, R. A.; Ymén, I. *Solid State Characterization of Pharmaceuticals*; Wiley: Chichester, 2012.
(4) Bernstein, J. *Cryst. Growth Des.* **2011**, *11*, 632−650.
(5) Bernstein, J. *Polymorphism in Molecular Crystals*; Clarendon Press: Oxford, 2002.
(6) Llinas, A.; Goodman, J. M. *Drug Discovery Today* **2008**, *13*, 198−210.
(7) Braun, D. E.; Karamertzanis, P. G.; Arlin, J. B.; Florence, A. J.; Kahlenberg, V.; Tocher, D. A.; Griesser, U. J.; Price, S. L. *Cryst. Growth Des.* **2011**, *11*, 210−220.
(8) Braun, D. E.; Bhardwaj, R. M.; Florence, A. J.; Tocher, D. A.; Price, S. L. *Cryst. Growth Des.* **2013**, *13*, 19−23.
(9) Stephenson, G. A.; Kendrick, J.; Wolfangel, C.; Leusen, F. J. *Cryst. Growth Des.* **2012**, *12*, 3964−3976.
(10) Kendrick, J.; Stephenson, G. A.; Neumann, M. A.; Leusen, F. J. *Cryst. Growth Des.* **2013**, *13*, 581−589.
(11) Gorbitz, C. H.; Dalhus, B.; Day, G. M. *Phys. Chem. Chem. Phys.* **2010**, *12*, 8466−8477.
(12) Braun, D. E.; Ardid-Candel, M.; D'Oria, E.; Karamertzanis, P. G.; Arlin, J. B.; Florence, A. J.; Jones, A. G.; Price, S. L. *Cryst. Growth Des.* **2011**, *11*, 5659−5669.
(13) Braun, D. E.; Bhardwaj, R. M.; Arlin, J. B.; Florence, A. J.; Kahlenberg, V.; Griesser, U. J.; Tocher, D. A.; Price, S. L. *Cryst. Growth Des.* **2013**, *13*, 4071−4083.
(14) Braun, D. E.; Karamertzanis, P. G.; Price, S. L. *Chem. Commun.* **2011**, *47*, 5443−5445.
(15) Cruz-Cabeza, A. J.; Day, G. M.; Jones, W. *Chem.—Eur. J.* **2008**, *14*, 8830−8836.
(16) Cruz-Cabeza, A. J.; Karki, S.; Fabian, L.; Friscic, T.; Day, G. M.; Jones, W. *Chem. Commun.* **2010**, *46*, 2224−2226.
(17) Bardwell, D. A.; Adjiman, C. S.; Arnautova, Y. A.; Bartashevich, E.; Boerrigter, S. X.; Braun, D. E.; Cruz-Cabeza, A. J.; Day, G. M.; la Valle, R. G.; Desiraju, G. R.; van Eijck, B. P.; Facelli, J. C.; Ferraro, M. B.; Grillo, D.; Habgood, M.; Hofmann, D. W.; Hofmann, F.; Jose, K. V.; Karamertzanis, P. G.; Kazantsev, A. V.; Kendrick, J.; Kuleshova, L. N.; Leusen, F. J.; Maleev, A. V.; Misquitta, A. J.; Mohamed, S.; Needs, R. J.; Neumann, M. A.; Nikylov, D.; Orendt, A. M.; Pal, R.; Pantelides, C. C.; Pickard, C. J.; Price, L. S.; Price, S. L.; Scheraga, H. A.; van de Streek, J.; Thakur, T. S.; Tiwari, S.; Venuti, E.; Zhitkov, I. K. *Acta Crystallogr., Sect. B* **2011**, *67*, 535−551.
(18) Kazantsev, A. V.; Karamertzanis, P. G.; Adjiman, C. S.; Pantelides, C. C.; Price, S. L.; Galek, P. T.; Day, G. M.; Cruz-Cabeza, A. J. *Int. J. Pharm.* **2011**, *418*, 168−178.
(19) Bhardwaj, R. M.; Price, L. S.; Price, S. L.; Reutzel-Edens, S. M.; Miller, G. J.; Oswald, I. D. H.; Johnston, B.; Florence, A. J. *Cryst. Growth Des.* **2013**, *13*, 1602−1617.
(20) Ismail, S. Z.; Anderton, C. L.; Copley, R. C.; Price, L. S.; Price, S. L. *Cryst. Growth Des.* **2013**, *13*, 2396−2406.
(21) Zeidan, T. A.; Trotta, J. T.; Chiarella, R. A.; Oliveira, M. A.; Hickey, M. B.; Almarsson, O.; Remenar, J. F. *Cryst. Growth Des.* **2013**, *13*, 2036−2046.
(22) Sun, C. C. *J. Pharm. Sci.* **2009**, *98*, 1744−1749.
(23) Experimental information about ionization state and Z' was already available and taken into consideration when setting up the CSP searches (see also Supporting Information section 1).
(24) Allen, F. H. *Acta Crystallogr., Sect. B* **2002**, *58*, 380−388.
(25) Karamertzanis, P. G.; Pantelides, C. C. *Mol. Phys.* **2007**, *105*, 273−291.
(26) Vasileiadis, M.; Kazantsev, A. V.; Karamertzanis, P. G.; Adjiman, C. S.; Pantelides, C. C. *Acta Crystallogr., Sect. B* **2012**, *68*, 677−685.
(27) Kazantsev, A. V.; Karamertzanis, P. G.; Adjiman, C. S.; Pantelides, C. C. *J. Chem. Theory Comput.* **2011**, *7*, 1998−2016.
(28) Karamertzanis, P. G.; Kazantsev, A. V.; Issa, N.; Welch, G. W. A.; Adjiman, C. S.; Pantelides, C. C.; Price, S. L. *J. Chem. Theory Comput.* **2009**, *5*, 1432−1448.
(29) Price, S. L.; Leslie, M.; Welch, G. W. A.; Habgood, M.; Price, L. S.; Karamertzanis, P. G.; Day, G. M. *Phys. Chem. Chem. Phys.* **2010**, *12*, 8478−8490.
(30) Stone, A. J. *J. Chem. Theory Comput.* **2005**, *1*, 1128−1132.
(31) Coombes, D. S.; Price, S. L.; Willock, D. J.; Leslie, M. *J. Phys. Chem.* **1996**, *100*, 7352−7360.
(32) Cossi, M.; Scalmani, G.; Rega, N.; Barone, V. *J. Chem. Phys.* **2002**, *117*, 43−45.
(33) Cooper, T. G.; Hejczyk, K. E.; Jones, W.; Day, G. M. *J. Chem. Theory Comput.* **2008**, *4*, 1795−1805.

(34) Day, G. M.; Cooper, T. G. *CrystEngComm* **2010**, *12*, 2443−2453.
(35) Anghel, A. T.; Day, G. M.; Price, S. L. *CrystEngComm* **2002**, *4*, 348−355.
(36) Day, G. M.; Price, S. L.; Leslie, M. *Cryst. Growth Des.* **2001**, *1*, 13−27.
(37) Day, G. M.; Price, S. L.; Leslie, M. *J. Phys. Chem. B* **2003**, *107*, 10919−10933.
(38) Gavezzotti, A. *J. Phys. Chem. B* **2002**, *106*, 4145−4154.
(39) Gavezzotti, A. *J. Phys. Chem. B* **2003**, *107*, 2344−2353.
(40) Gavezzotti, A. *New J. Chem.* **2011**, *35*, 1360−1368.
(41) Clark, S. J.; Segall, M. D.; Pickard, C. J.; Hasnip, P. J.; Probert, M. J.; Refson, K.; Payne, M. C. *Z. Kristallogr.* **2005**, *220*, 567−570.
(42) Perdew, J. P.; Burke, K.; Ernzerhof, M. *Phys. Rev. Lett.* **1996**, *77*, 3865−3868.
(43) Vanderbilt, D. *Phys. Rev. B* **1990**, *41*, 7892−7895.
(44) Tkatchenko, A.; Scheffler, M. *Phys. Rev. Lett.* **2009**, *102*, 073005−1−073005/4.
(45) Grimme, S. *J. Comput. Chem.* **2006**, *27*, 1787−1799.
(46) Macrae, C. F.; Bruno, I. J.; Chisholm, J. A.; Edgington, P. R.; McCabe, P.; Pidcock, E.; Rodriguez-Monge, L.; Taylor, R.; van de Streek, J.; Wood, P. A. *J. Appl. Crystallogr.* **2008**, *41*, 466−470.
(47) Gelbrich, T.; Threlfall, T. L.; Hursthouse, M. B. *CrystEngComm* **2012**, *14*, 5454−5464.
(48) *SAINT: Program for Integration of Area Detector Data*, version 6.2; Bruker AXS: Madison WI, USA, 2001.
(49) Farrugia, L. *J. Appl. Crystallogr.* **1999**, *32*, 837−838.
(50) Burla, M. C.; Caliandro, R.; Camalli, M.; Carrozzini, B.; Cascarano, G. L.; De Caro, L.; Giacovazzo, C.; Polidori, G.; Spagna, R. *J. Appl. Crystallogr.* **2005**, *38*, 381−388.
(51) Sheldrick, G. M. *Acta Crystallogr., Sect. A.* **2008**, *64*, 112−122.
(52) Fung, B. M.; Khitrin, A. K.; Ermolaev, K. *J. Magn. Reson.* **2000**, *142*, 97−101.
(53) Antzutkin, O. N. *Prog. Nucl. Magn. Reson. Spectrosc.* **1999**, *35*, 203−266.
(54) Metz, G.; Wu, X. L.; Smith, S. O. *J. Magn. Reson. A* **1994**, *110*, 219−227.
(55) Braun, D. E.; McMahon, J. A.; Koztecki, L. H.; Price, S. L.; Reutzel-Edens, S. M. *In preparation*, 2014
(56) Sheth, A. R.; Zhou, D.; Muller, F. X.; Grant, D. J. W. *J. Pharm. Sci.* **2004**, *93*, 3013−3026.
(57) Puigjaner, C.; Barbas, R.; Portell, A.; Font-Bardia, M.; Alcobe, X.; Prohens, R. *Cryst. Growth Des.* **2010**, *10*, 2948−2953.
(58) Price, S. L. *Acta Crystallogr., Sect. B* **2013**, *69*, 313−328.
(59) Price, S. L. *Chem. Soc. Rev.* **2014**, *43* (7), 2098−2111.
(60) A double layer of SC DB7-GG1 leads to DB7-2GG1.
(61) Markvardsen, A. J.; David, W. I. F.; Johnson, J. C.; Shankland, K. *Acta Crystallogr., Sect. A* **2001**, *57*, 47−54.
(62) David, W. I. F.; Shankland, K.; van de Streek, J.; Pidcock, E.; Motherwell, W. D. S.; Cole, J. C. *J. Appl. Crystallogr.* **2006**, *39*, 910−915.
(63) Spek, A. L. *J. Appl. Crystallogr.* **2003**, *36*, 7−13.
(64) Habgood, M.; Grau-Crespo, R.; Price, S. L. *Phys. Chem. Chem. Phys.* **2011**, *13*, 9590−9600.
(65) Braun, D. E.; Kahlenberg, V.; Gelbrich, T.; Ludescher, J.; Griesser, U. J. *CrystEngComm* **2008**, *10*, 1617−1625.
(66) Burger, A.; Ramberger, R. *Mikrochim. Acta* **1979**, *2*, 273−316.
(67) Otero-de-la-Roza, A.; Johnson, E. R. *J. Chem. Phys.* **2012**, 137.
(68) Dunitz, J.; Gavezzotti, A. *J. Phys. Chem. B* **2012**, *116*, 6740−6750.
(69) The prior knowledge of the structure of Form I DB7 was essential for expanding the range of structures to be analyzed. This can be seen as a combination of the errors in the relative energies in the method used in the search (Figure 17) and the need to gain experience of this type of molecule.
(70) Childs, S. L.; Wood, P. A.; Rodriguez-Hornedo, N.; Reddy, L. S.; Hardcastle, K. I. *Cryst. Growth Des.* **2009**, *9*, 1869−1888.
(71) Wood, P. A.; Olsson, T. S.; Cole, J. C.; Cottrell, S. J.; Feeder, N.; Galek, P. T.; Groom, C. R.; Pidcock, E. *CrystEngComm* **2013**, *15*, 65−72.
(72) Galek, P. T. A.; Pidcock, E.; Wood, P. A.; Bruno, I. J.; Groom, C. R. *CrystEngComm* **2012**, *14*, 2391−2403.
(73) Cruz-Cabeza, A. J.; Day, G. M.; Jones, W. *Chem.—Eur. J.* **2009**, *15*, 13033−13040.
(74) Wu, H.; Habgood, M.; Parker, J. E.; Reeves-McLaren, N.; Cockcroft, J. K.; Vickers, M.; West, A. R.; Jones, A. G. *CrystEngComm* **2013**, *15*, 1853−1859.
(75) Mohamed, S.; Tocher, D. A.; Price, S. L. *Int. J. Pharm.* **2011**, *418*, 187−198.
(76) Braun, D. E.; Tocher, D. A.; Price, S. L.; Griesser, U. J. *J. Phys. Chem. B* **2012**, *116*, 3961−3972.
(77) Habgood, M.; Lancaster, R. W.; Gateshki, M.; Kenwright, A. M. *Cryst. Growth Des.* **2013**, *13*, 1771−1779.
(78) Bauer, J.; Spanton, S.; Henry, R.; Quick, J.; Dziki, W.; Porter, W.; Morris, J. *Pharm. Res.* **2001**, *18*, 859−866.
(79) Gelbrich, T.; Braun, D. E.; Ellern, A.; Griesser, U. J. *Cryst. Growth Des.* **2013**, *13*, 1206−1217.
(80) Huang, Y.; Shao, Y.; Beran, G. J. *J. Chem. Phys.* **2013**, 138.
(81) Marom, N.; DiStasio, R. A.; Atalla, V.; Levchenko, S.; Reilly, A. M.; Chelikowsky, J. R.; Leiserowitz, L.; Tkatchenko, A. *Angew. Chem., Int. Ed.* **2013**, *52*, 6629−6632.
(82) Barnett, S. A.; Johnson, A.; Florence, A. J.; Price, S. L.; Tocher, D. A. *Cryst. Growth Des.* **2008**, *8*, 24−36.
(83) Arlin, J. B.; Price, L. S.; Price, S. L.; Florence, A. J. *Chem. Commun.* **2011**, *47*, 7074−7076.
(84) Zencirci, N.; Gelbrich, T.; Kahlenberg, V.; Griesser, U. J. *Cryst. Growth Des.* **2009**, *9*, 3444−3456.
(85) Fabbiani, F. P. A.; Allan, D. R.; David, W. I. F.; Davidson, A. J.; Lennie, A. R.; Parsons, S.; Pulham, C. R.; Warren, J. E. *Cryst. Growth Des.* **2007**, *7*, 1115−1124.
(86) Stahly, G. P. *Cryst. Growth Des.* **2007**, *7*, 1007−1026.
(87) Abramov, Y. A. *Org. Process Res. Dev.* **2013**, *17*, 472−485.